Chapter 9
Multi-Objective Supervisory Controller for Hybrid Electric Vehicles

Stefano Marelli and Simona Onori

Abstract In this article, we address the problem of energy management control design in hybrid electric vehicles (HEVs) to achieve minimum fuel consumption while optimally limiting battery degradation. We use Pontryagin's minimum principle (PMP) to solve the optimal control problem. To the end of controlling battery aging to guarantee battery performances over 150,000 miles, a battery capacity loss reference trajectory is defined and a battery aging model is used by the optimizer. The resulting optimal supervisory control strategy is able to regulate both state of charge and capacity loss to their reference values. Simulation results conducted on a pre-transmission HEV show that the battery capacity loss can be regulated to achieve the long-term objective without sacrificing much fuel economy.

Keywords Electric vehicles • Supervisory control • Multi-objective

9.1 Introduction

Battery aging plays an important role in hybrid electric vehicles (HEVs) performance: if not properly controlled, faster battery degradation leads to lower energy recovery and lower power output capacity, requiring the battery early replacement and causing a reduction in the HEV monetary saving. A hybrid vehicle has two (or more) sources of energy on-board, whose operation is coordinated by an energy management system (EMS) typically in a way that minimum fuel consumption is achieved [1–3]. Realistic figures of achievable improvement in fuel economy in HEVs range from 10 % for mild hybrids to more than 30 % for highly hybridized vehicles. This potential can be realized only with a sophisticated control system that optimizes energy flows within the vehicle. This consideration has spurred a considerable amount of research in the last 15 years towards *model-based optimal supervisory control techniques* moving away from heuristic or rule-based methods. Systematic model-optimization methods such as dynamic programming (DP) and

S. Marelli • S. Onori (✉)
Department of Automotive Engineering, Clemson University, International Center for Automotive Research, Greenville, SC 29607, USA
e-mail: stefano.marelli.engineer@gmail.com; sonori@clemson.edu

Q. Zhang et al., *Automotive Air Conditioning*, DOI 10.1007/978-3-319-33590-2_9

Pontryagin's minimum principle (PMP) have been successfully adopted to design controllers to improve the energy management in HEVs using meaningful objective functions [4–9].

These optimal control techniques are referred to as *non-causal*, in that their solution relies on a perfect knowledge of the driving cycle, and as such not implementable in real-time. Nonetheless, they are useful for two reasons: (i) they can be used to understand how an optimal solution works, from which rules can be extracted to design real-time implementable control strategies [10], (ii) they can be used to benchmark realizable strategies. For a more comprehensive overview of different control methods developed for HEVs, the reader can refer to [5].

Traditionally, the HEV energy management problem was formulated with the aim of minimizing fuel consumption (or emissions, [11]) while trying to guarantee a charge-sustaining operation of the battery. No considerations about battery use (or misuse) were included in the original problem formulation. Only recently, though, industry has become more concerned about efficiently managing the energy on-board HEVs and, at the same time, monitoring and controlling the battery degradation. If a model-based optimization approach has to be taken to this regards in order to systematically include battery deterioration concerns within the problem formulation, an aging model of the battery is needed. In fact, the study conducted at Argonne National Laboratory [12] showed that the best monetary savings in HEVs are obtained when the battery life matches the vehicle life. Battery End Of Life (EOL) is generally defined as the point in time when battery capacity reduces to 80 % of its initial value [12]. If the goal is to make the vehicle life (usually 150, 000 mi or 15 years) match the battery life, this translates into achieving a 20 % capacity degradation over 150, 000 mi, thus avoiding battery early replacement.

Only over the past few years, optimal supervisory control methods have included aging considerations. One of the first works in this vein is [13] that proposes a cost function that is a convex combination of instantaneous energy (fuel and electricity) and aging costs (given in terms of solid electrolyte interphase layer growth) and solves the problem via stochastic dynamic programming (SDP) for plug-in hybrid electric vehicles (PHEVs). In [14] a PMP-based solution is proposed where a convex combination of fuel and aging cost is used in the cost function; in this case, the capacity loss in HEV is being minimized. A weighting coefficient was used in the cost function to generate a family of Pareto front solutions. A similar approach is followed in [15], where the cost function proposed by [14] is normalized to simplify the physical interpretation of the control parameters.

These latter works tried to minimize the battery deterioration without any explicit goal on battery life duration. The first attempt to achieve such an objective is found in [16]. A battery aging model from [17] is used in the problem formulation, and a PMP-based solution is presented based on a two-state model (state of charge and capacity loss). A solution of the PMP problem was not given, rather an approximate solution based on extending the adaptation law, used in [10], to the two costates was presented, based on the simplistic assumption that the capacity loss trend over the

vehicle life span is linear. In [18] an adaptive version of PMP is proposed as well, to minimize fuel consumption and battery aging, while limiting battery temperature. Qualitative results were presented for rather limited conditions of operation.

The objective of this paper is to use an experimentally validated battery aging model into the EMS, to systematically control capacity degradation during the operational life of the vehicle, with a minimum impact on the vehicle performances. The problem of fuel consumption minimization and battery degradation limitation for HEVs is inherently a *two-time scale* control problem in that nominally the two objectives have to be reached over two different time horizons: driving cycle and battery life, respectively. In fact, we normally test vehicles performance over standard driving cycles while battery life is measured in terms of total ampere-hours throughput. The proposed optimal supervisory control strategy is able to reduce the two-time scale problem to a one-time scale problem, by minimizing an instantaneous cost function and guaranteeing a predefined battery degradation trend on a short-time horizon, leading to 20 % cumulative capacity loss over 150, 000 mi.

In this manuscript, we first use an experimentally validated battery aging model from [19] to monitor and control degradation within the multi-objective optimal control framework. We then express the costate dynamics of PMP, including the dependence of the mass fuel flow rate of the engine from the state of charge of the battery. Third, we formulate an aging limiting control problem with two states which requires a capacity loss reference trajectory to be defined. In this way, the multi-objective supervisory control problem (hereinafter referred to as "aging-limiting PMP" problem) is solved as a regulation problem on the two states (state of charge and capacity). The aging-limiting PMP (AL-PMP) problem is finally solved by proposing a novel analytic/numerical methodology along with a tuning algorithm. An analytic comparison between the newly proposed AL-PMP problem and the optimization presented in [1] is shown, and a new interpretation of the well-known ECMS strategy, extended to the case with battery aging, is proposed.

The paper is organized as follows: in Sect. 9.2 the adopted aging model is presented, and the capacity loss reference trajectory is defined; in Sect. 9.3 the vehicle simulator is presented, and a focus is put on the battery cell and pack model including aging; in Sect. 9.4 the meaningfulness of the control problem is explained and two situations are defined; in Sect. 9.5 the aging-limiting optimal control problem is formulated, and it is solved with AL-PMP in Sect. 9.6; in Sect. 9.7 the novel control strategy is compared with other two different approaches, which show to be equivalent to AL-PMP, but more problematic in the implementation; in Sect. 9.8 the penalty function on battery capacity loss is shown and analyzed; in Sect. 9.9 AL-PMP is optimally tuned and simulation results are shown in Sect. 9.10; finally, conclusions are given in Sect. 9.11.

9.2 Battery Aging Model and Capacity Loss Reference Trajectory

Aging is an irreversible process caused by parasitic chemical reactions that take place inside the battery. Batteries can undergo two types of aging: *calendar aging* [20, 21] and *cycle-life aging* [17, 19, 22]. In this paper only cycle-life aging is being addressed, and an empirical capacity degradation model is used in the control strategy.

The factors responsible for battery aging are usually referred to as *severity factors* [23]. In HEV applications, those are typically: state of charge, SOC, C-rate, defined as $I_c = I/Q$ (where I is the battery current in $[A]$ and Q is the actual capacity in $[Ah]$), and battery internal temperature, θ. The capacity loss model, from [19], is identified on real HEV battery data with a complete dependence on severity factors by means of a *severity factor function*, σ_{funct}. The following functional relationship exists between σ_{funct} and Q_{loss}:

$$Q_{\text{loss}}(SOC, I_c, \theta, Ah) = \sigma_{\text{funct}}(SOC, I_c, \theta) \cdot Ah^z \tag{9.1}$$

where Q_{loss} is the percent capacity loss, defined as $Q_{\text{loss}} = (1 - Q/Q_0) \cdot 100$, where Q_0 is the initial capacity in $[Ah]$; z is an empirical power exponent; and Ah is the accumulated ampere-hour throughput of the battery, given by $Ah = \int_0^t \frac{|I|}{3600} d\tau$. SOC is expressed as a fraction, I_c is in $[1/h]$ and θ is in [°C]. The severity factor function assumes the following form:

$$\sigma_{\text{funct}}(SOC, I_c, \theta) = (\alpha\, SOC + \beta) \cdot exp\left(\frac{-E_a + \eta\ |I_c|}{R_g\,(273.15 + \theta)}\right) \tag{9.2}$$

where α, β and η are model parameters (identified in [19]), E_a is the activation energy in $[J/mol]$ and R_g is the universal gas constant in $[J/mol/K]$.

In this work, the control-oriented severity factor map, σ_{map}, originally defined in [14] for PHEVs and then further refined for HEV batteries in [19], is considered. It is defined as the ratio of the total Ah-throughput under nominal conditions until EOL is reached (i.e., Γ) to the total Ah-throughput under actual operating conditions (i.e., γ):

$$\begin{aligned} \sigma_{\text{map}}(SOC, I_c, \theta) &= \frac{\Gamma\,(SOC_{\text{nom}}, I_{c,\text{nom}}, \theta_{\text{nom}})}{\gamma\,(SOC, I_c, \theta)} \\ &= \frac{\int_0^{t_{\text{EOL}}} |I_{\text{nom}}|\, d\tau}{\int_0^{t_{\text{EOL}}} |I|\, d\tau} \end{aligned} \tag{9.3}$$

where SOC_{nom}, $I_{c,\text{nom}}$, θ_{nom}, and I_{nom} represent predefined nominal operating conditions and t_{EOL} is the time at EOL. The severity factor map is a measure of the relative aging effect on the battery at a given operating condition with respect to

the nominal operation. It can be used the same way as an engine fuel consumption map, in that it allows to select the battery operating points in the domain (SOC, I_c, θ) to ensure lower capacity degradation. The capacity loss model (9.1), together with the severity factor function (9.2) is used in the following to capture battery aging dynamics and estimate the actual capacity, as described in Sect. 9.3.1.3. The severity factor map, on the other hand, is used in the EMS by the optimizer to select the optimal battery operating points to limit its aging, as described in Sect. 9.6.

9.2.1 Capacity Loss Reference for Cycle-Life

Since the electrochemical aging processes that take place inside the battery are irreversible, the capacity loss is a monotonically increasing function of *Ah*-throughput, as it can only increase if the battery is being used (or stay constant if the battery is not being used). In this paper, we define a capacity loss reference trajectory, with the purpose of limiting capacity loss over each day of driving. In particular, the capacity loss reference is expressed as a function of the driven distance d (expressed in miles, $[mi]$), and average severity factor values are used in σ_{funct} for (9.1). Simulations performed over US06 and FUDS driving cycles at ambient temperatures of $\theta_{\text{amb}} = 20$, 30 and 40°C produce the average values reported in Table 9.1. In addition, a scaling factor, K, is introduced, resulting in:

$$Q_{\text{loss,ref}}(d) = K \cdot \sigma_{\text{funct}}\left(\overline{SOC}, \overline{I}_c, \overline{\theta}\right) \cdot d^z \tag{9.4}$$

where z is from (9.1). K is selected to ensure that 20 % capacity loss is reached after 150, 000 mi, as follows:

$$K = \frac{Q_{\text{loss,EOL}}}{\sigma_{\text{funct}}\left(\overline{SOC}, \overline{I}_c, \overline{\theta}\right) \cdot d_{\text{EOL}}^z} \tag{9.5}$$

where the EOL capacity loss and traveled distance are $Q_{\text{loss,EOL}} = 20\,\%$ and $d_{\text{EOL}} = 150,000mi$, respectively, resulting in $K = 0.6837$. Figure 9.1 shows the capacity loss reference as a function of the driven distance until the distance d_{EOL} is reached.

The *two-time scale* optimal control problem is reduced to a single time scale problem by means of breaking up d_{EOL} into intervals of single days of driving, over which a daily capacity loss reference value is defined. Statistics shows that a typical

Table 9.1 Average severity factor values used in the capacity loss reference

Parameter	Value
$\overline{SOC}[-]$	0.446
$\overline{I}_c[1/h]$	2.43
$\overline{\theta}[°C]$	36.1

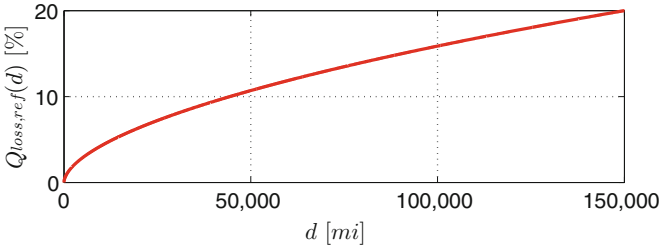

Fig. 9.1 Capacity loss reference based on driven distance

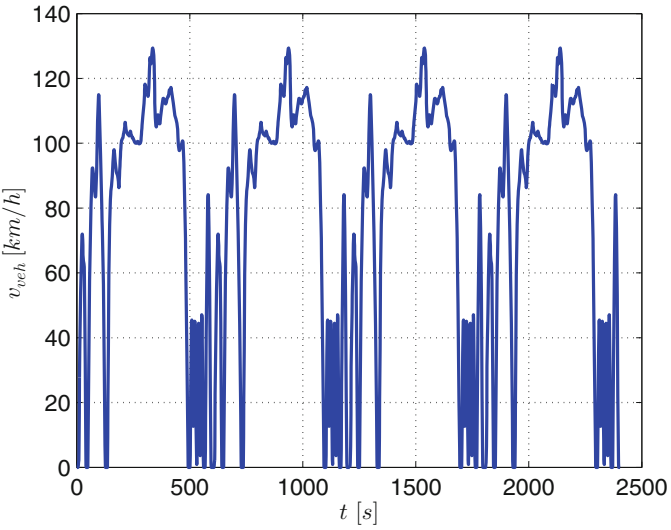

Fig. 9.2 Vehicle speed profile resulting from linking 4 US06 driving cycles

daily trip for a US car driver is estimated to be 28.97*mi* [24]. To account for this statistics, in this work, one day of driving is defined as the concatenation of four US06 or four FUDS driving cycles, resulting in a total distance driven in one day of $d_f = 32.14mi$ and $d_f = 30.02mi$, respectively. The two one-day speed profiles are shown in Figs. 9.2 and 9.3.

The daily Q_{loss} reference is computed from the overall capacity reference trajectory (9.4), over the daily distance traveled. The target value of capacity loss at the end of a generic day k (with $k \in \mathbb{N},\ k \leq k_{\text{EOL}}$, where k_{EOL} is the last day before battery EOL is reached) is obtained evaluating $Q_{\text{loss,ref}}(d)$ at $d = kd_f$. Figure 9.4 shows the quantity just defined, for the first three days of US06 driving cycles.

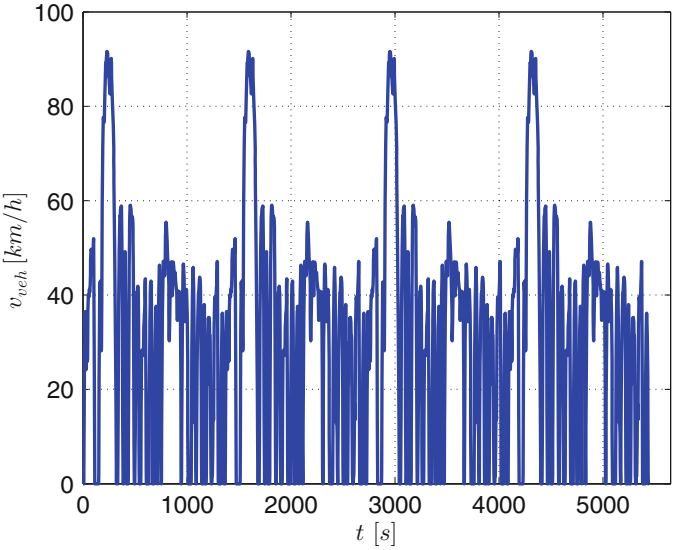

Fig. 9.3 Vehicle speed profile resulting from linking 4 FUDS driving cycles

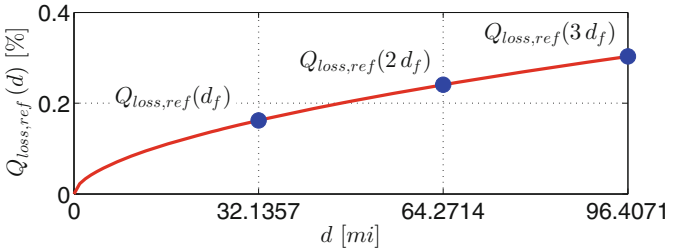

Fig. 9.4 Daily capacity loss reference points calculated from US06 driving cycles, for which $d_f = 32.1357mi$

9.3 Vehicle Simulator

The vehicle simulator used in this work is an improved version of the one developed in [15] that models the parallel pre-transmission Hybrid Honda Civic. The main characteristics of the vehicle are listed in Table 9.2 and its layout is shown in Fig. 9.5. It comprises an integrated motor assist (IMA) where the electric motor (EM) is mounted on the same shaft of the internal combustion engine (ICE). A continuous variable transmission (CVT) allows the vehicle to operate in (i) conventional, (ii) full-electric, (iii) power-assist, or (iv) recuperation mode. In the first mode of operation, only the ICE is running and supplies all the power requested by the driver. In the second mode, only the EM is running, and the engine is switched off. In power-assist mode, the EM and the ICE are running in parallel and the power

Table 9.2 Hybrid Honda Civic vehicle model characteristics used in the simulator

Component	Specifications
Vehicle mass	$1294kg$
ICE	$1.6l$, 85kW
	In-line 4-cylinders
	Gasoline
EM	Maximum peak power $30kW$
	Maximum continuous power $15kW$
CVT	Ratio 0.529–3.172
	Final drive 3.94
Battery pack	$LiFePO_4$
	Nominal capacity $4.6Ah$ ($803Wh$)
	Maximum power $20kW$

Fig. 9.5 Vehicle layout

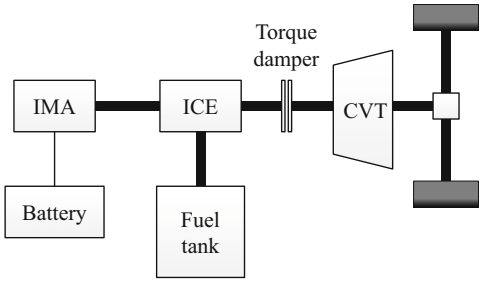

is split between the two, according to the supervisory control strategy. Finally, in recuperation mode, the EM is used to send all the braking power into the battery for energy recuperation; if the saturation limits of the EM or of the battery are reached, the remaining part of the braking power is transferred to the friction brakes, according to a series braking control strategy [25]. The CVT allows a smooth transition between the four modes of operation.

A quasi-static energy-based forward modeling approach is used to simulate the longitudinal dynamics of the hybrid vehicle [1], whose structure is shown in Fig. 9.6. A driver model converts the error between the driving cycle desired speed and the actual vehicle speed into the requested power P_{req}, which is sent to the Supervisory controller, along with ICE speed, ω_{ice}, EM speed ω_{em}, and SOC to generate the optimal actuators set points used in the Powertrain module. The actual vehicle velocity is obtained in the Vehicle dynamics block by integration of the longitudinal vehicle dynamics equation. The vehicle components, ICE and EM are modeled by means of their efficiency maps [15].

The improvements introduced in the simulator for the scope of the present work are related to the battery model, both in the Powertrain and in the Supervisory controller modules. Battery aging dynamics are modeled in the Powertrain model, whereas the formulation of a new instantaneous cost inside the Supervisory controller makes use of the severity factor map, as described in Sect. 9.6.

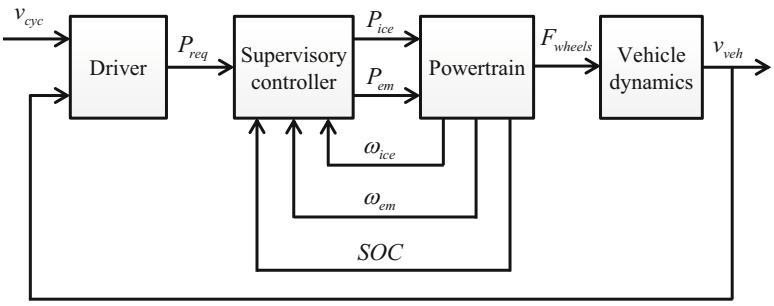

Fig. 9.6 Vehicle simulator block diagram

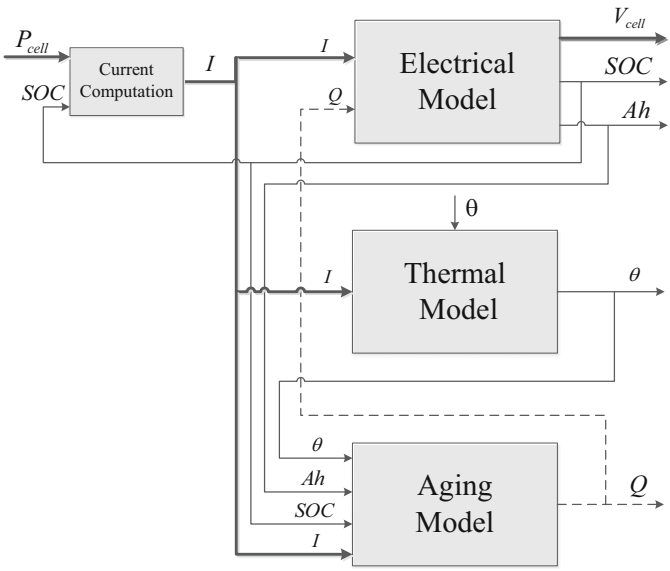

Fig. 9.7 Battery model layout: electrical, thermal, and aging dynamics and their interconnections

9.3.1 Battery Cell Model

In this work an ANR26650 $LiFePO_4$ battery system from A123 is considered, which has a nominal capacity of $2.3Ah$ and a nominal voltage of $3.3V$. The battery cell model is composed of three components: electrical, thermal, and aging, as depicted in Fig. 9.7. For each of these components, all the dynamics involved and their mutual effects are analyzed in the following. The battery pack model is then obtained by scaling up the cell parameters at pack level, according to the topology of the pack used.

9.3.1.1 Electrical Model

The electrical battery cell behavior is modeled with a 0th-order Randle's model. The input to the battery cell is the power, P_{cell}. The corresponding current is computed through the non-linear algebraic function [26]:

$$I = \frac{V_{\text{oc}}(SOC) - \sqrt{V_{\text{oc}}^2(SOC) - 4R_0(SOC,\theta)P_{\text{cell}}}}{2R_0(SOC,\theta)} \tag{9.6}$$

where I is positive in discharge, V_{oc} in $[V]$ is the cell open circuit voltage, which is a non-linear function of SOC, and R_0, in general a function of SOC and θ, is the cell internal resistance at the Beginning Of Life BOL. Figure 9.8 shows a typical trend of the resistance as a function of SOC parameterized for different values of temperature θ [27].
The SOC cell dynamics are defined by the equation:

$$\dot{SOC} = -\frac{I}{3600\, Q_0(\theta)} \tag{9.7}$$

where Q_0, the BOL capacity, is a function of θ as shown in Fig. 9.9.

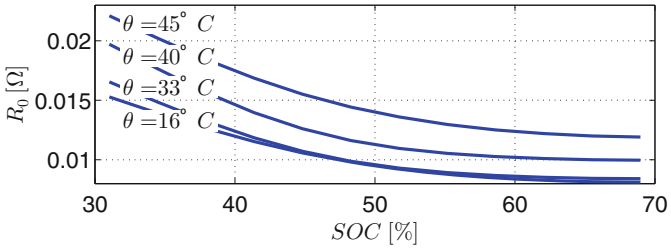

Fig. 9.8 Experimental characterization of R_0 as a function of SOC and θ for A123 ANR26650 battery cell

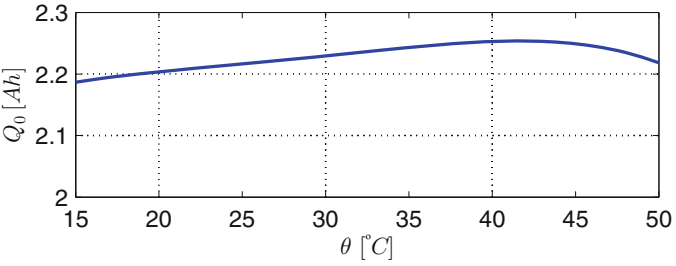

Fig. 9.9 Experimental characterization of Q_0 as a function of θ for A123 ANR26650 battery cell

As the battery is used, it ages. For, Q_0 must be updated with its actual value Q during vehicle operation. The increase in internal resistance due to aging is neglected in this work, and left as a future work.

The terminal voltage V_{cell} is given by

$$V_{\text{cell}} = V_{\text{oc}}(SOC) - R_0(SOC, \theta)\, I \tag{9.8}$$

and the cell power input is given by $P_{\text{cell}} = V_{\text{cell}}\, I$.

9.3.1.2 Thermal Model

The cell thermal model describes the cell temperature dynamics, taking into account the internal heat generation due to the current flowing inside the cell and the heat exchanged with the environment. The dynamics of the cell core temperature θ are described by the equation:

$$\dot{\theta} = \frac{1}{M_c C_p}\left[R_0(SOC, \theta)\, I^2 - \frac{\theta - \theta_{\text{amb}}}{R_u}\right] \tag{9.9}$$

where $R_0\, I^2$ in $[W]$ is the thermal power generated by Joule effect, $M_c C_p$ in $[J/°\text{C}]$ is the effective cell heat capacity, considered constant, θ_{amb} in $[°\text{C}]$ is the ambient temperature, and R_u is the thermal resistance to model the cell heat exchange with the environment. The parameter values of the first-order model used to simulate (9.9) are given in [28].

9.3.1.3 Aging Model

In order to define the capacity loss dynamics, we take the derivative of (9.1) with respect to time. Since the data used for the model identification are collected from tests conducted under SOC, I_c, and θ constant conditions, when computing the time derivative of Q_{loss}, σ_{funct} is considered as a constant. Thus $\frac{dQ_{\text{loss}}}{dt} = \frac{\partial Q_{\text{loss}}}{\partial Ah}\frac{\partial Ah}{\partial t}$, which leads to

$$\dot{Q}_{\text{loss}} = \sigma_{\text{funct}}(SOC, I_c, \theta)\, z \cdot Ah^{z-1} \cdot \dot{Ah} \tag{9.10}$$

The aging model (9.10) is integrated in the powertrain module to obtain the actual value of Q_{loss}. This is then used in the EMS to solve the multi-objective optimal control problem.

9.3.2 Battery Pack Model

The battery pack used in the vehicle is composed of $N_p = 2$ modules in parallel with $N_s = 54$ cells in series for each module. The battery pack quantities are computed, for the sake of simplicity, under the assumption that all the cells are equal and balanced, leading to a pack current of

$$I_{\text{batt}} = N_p\, I \tag{9.11}$$

a pack open circuit voltage of

$$V_{\text{oc,batt}} = N_s\, V_{\text{oc}} \tag{9.12}$$

and a terminal voltage of

$$V_{\text{batt}} = N_s\, V_{\text{cell}} \tag{9.13}$$

The battery pack power is given by

$$P_{\text{batt}} = N_p\, N_s\, P_{\text{cell}} \tag{9.14}$$

and the pack resistance by

$$R_{0,batt} = \frac{N_s}{N_p}\, R_0 \tag{9.15}$$

Moreover, the initial and actual pack capacities are:

$$Q_{0,batt} = N_p\, Q_0, \tag{9.16}$$

$$Q_{\text{batt}} = N_p\, Q \tag{9.17}$$

respectively.

9.4 Well-Posedness of Multi-Objective Control Problem

The aim of the multi-objective optimal control problem is to obtain minimum fuel consumption, while guaranteeing charge-sustainability and limited capacity degradation over a day of driving.

Because of the diverse nature of driving cycles (due to different terrains, drivers, weather conditions, etc.) the multi-objective optimal control problem is well defined (and meaningful) only for those cases where the driving conditions (in terms of severity factors: SOC and I_c) and/or ambient conditions (θ_{amb}) would lead to a

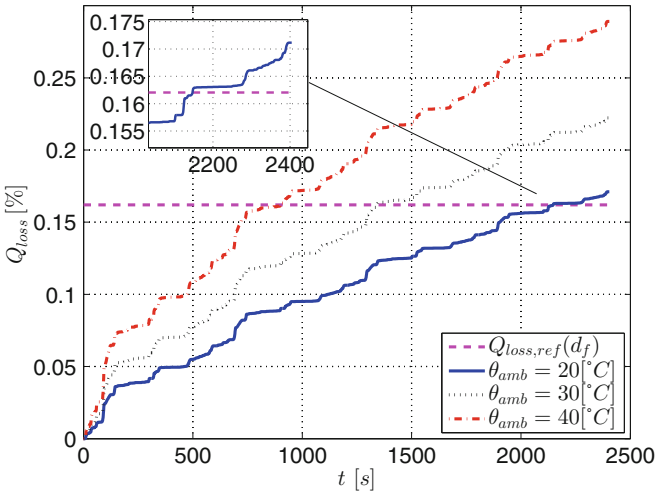

Fig. 9.10 Capacity loss over the first day (combination of 4 US06) of aggressive cycle for different ambient temperatures. Simulation results are obtained by controlling fuel consumption only (using the PMP method): capacity loss always exceeds the $Q_{\text{loss,ref}}(d_f)$ limit. If only fuel is minimized in the vehicle EMS, the battery will degrade (reaching EOL) prematurely

degradation of the battery beyond the acceptable target $Q_{\text{loss,ref}}(d_f)$. In this case, battery aging must be controlled. The US06 is one of such cycle, as shown in Fig. 9.10. In other cases, driving scenarios are inherently mild from an aging standpoint, in that they would never lead to a battery degradation close to the daily target value, as shown in Fig. 9.11 for the case of FUDS. Obviously, in such cases, battery aging does not have to be controlled, and the traditional fuel minimization problem can be employed.

Under aggressive cycles the EMS must monitor and limit the aging to meet the long-term goal of 20 % capacity loss over the vehicle life span to prevent anticipated battery degradation. Inclusion of a battery aging cost in the optimization problem is needed, at the price of slightly worsening in fuel economy. Under mild driving, operating in only fuel consumption minimization mode would be sufficient to guarantee a capacity loss below the target threshold.

The multi-objective optimal control problem is *well-posed* if the capacity degradation resulting from fuel consumption minimization exceeds its daily target limit. In this case, a multi-objective EMS is needed to optimally weigh fuel economy and battery aging.

The novel control strategy proposed in this work, referred to as *aging-limiting*, has the aim to control (limit) Q_{loss} (along with minimizing fuel consumption) to its daily target value $Q_{\text{loss,ref}}(d_f)$. Ideally, in a real-world scenario, a vehicle driving predictor would be used to interact with EMS. The EMS will then decide whether to switch to battery saving mode by activating the aging-limiting strategy or stay in the

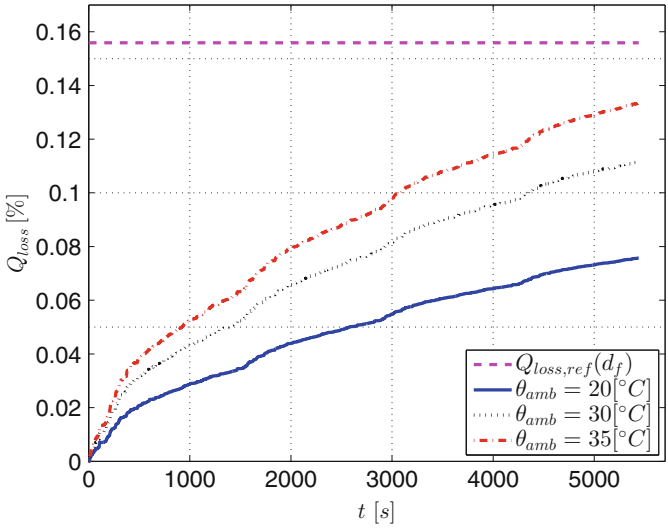

Fig. 9.11 Capacity loss over the first day (combination of 4 FUDS) of mild cycle for different ambient temperatures. Simulation results are obtained by controlling fuel consumption only (using the PMP method): capacity loss never exceeds the $Q_{\text{loss,ref}}(d_f)$ limit. In this specific cases, battery aging control is not needed

default fuel-consumption mode. The actual online strategy implementation is out of scope and will be investigated in the future.

In this work, we focus on the development of the new aging-limiting approach using US06 driving cycles as driving scenarios, for which the multi-objective control problem is well-posed.

9.5 Aging-Limiting Energy Management Problem Formulation

The aging-limiting control problem is formulated using the integral of the fuel power as cost function, as follows:

$$J(u, P_{\text{req}}) = \int_0^{t_f} \dot{m}_f(u, P_{\text{req}})\, Q_{\text{lhv}}\, dt \tag{9.18}$$

where u is the control input, i.e. the battery power $P_{\text{batt}} = I_{\text{batt}}\, V_{\text{batt}}$ in $[W]$ (positive in discharge); $\dot{m}_f$ is the mass fuel flow rate of the engine, in $[g/s]$; Q_{lhv} is the fuel lower heating value in $[J/g]$; and t_f is the final time instant in $[s]$, i.e. the duration of the driving day.

The goal of the aging-limiting supervisory controller is to find the optimal control sequence u^*, that minimizes (9.18) while (i) keeping SOC at the same reference value SOC_{ref} at the beginning and at the end of the driving day (9.19a), (ii) limiting the SOC excursion between fixed minimum and maximum values, respectively, $SOC_{\min}$ and $SOC_{\max}$ (9.19b), and (iii) controlling capacity loss to not exceed the target value (9.19c):

$$SOC(0) = SOC(t_f) = SOC_{\text{ref}} \tag{9.19a}$$

$$SOC_{\min} \leq SOC \leq SOC_{\max} \tag{9.19b}$$

$$0 \leq Q_{\text{loss}} \leq Q_{\text{loss,ref}}(d_f) \tag{9.19c}$$

The use of *power-based* cost function makes the choice of *depletion energy*, E_{dep} in $[J]$, to describe the battery dynamics, and the *effective energy-throughput*, E_{eff} in $[J]$, to describe battery aging dynamics, more practical as opposed to the traditionally used SOC and Q_{loss}. These quantities are defined as follows:

1. Depletion energy[1]:

$$\begin{aligned} x_1 = E_{\text{dep}} = \\ = E_{\text{dep}}(0) + \int_0^t I_{\text{batt}}(SOC, P_{\text{batt}}, \theta)\, V_{\text{oc,batt}}(SOC)\, d\tau \end{aligned} \tag{9.20}$$

   This state represents the amount of energy extracted from the battery pack and is equivalent to SOC in the control problem. Considering a negligible dependence of $V_{\text{oc,batt}}$ on SOC (typical in a charge-sustaining HEV), and a negligible variation of Q_{batt} over one day of driving, then the state of charge can be written as a function of E_{dep}[2]:

$$SOC = SOC(0) + \frac{E_{\text{dep}}(0) - E_{\text{dep}}}{3600\, Q_{\text{batt}}\, V_{\text{oc,batt}}} \tag{9.21}$$

2. Effective energy-throughput:

$$\begin{aligned} x_2 = E_{\text{eff}} = \int_0^t \sigma_{\text{map}}(SOC, I_c, \theta) \\ \cdot |I_{\text{batt}}(SOC, P_{\text{batt}}, \theta)|\, V_{\text{oc,batt}}(SOC)\, d\tau \end{aligned} \tag{9.22}$$

[1] The dependence on time will be left implicit in this paper, for simplicity.

[2] Under this assumption, it is possible to write (9.20) as $E_{\text{dep}} = E_{\text{dep}}(0) + V_{\text{oc,batt}} \int_0^t I_{\text{batt}}(SOC, P_{\text{batt}}, \theta)\, d\tau$ and the state of charge as $SOC = SOC(0) - \frac{1}{3600\, Q_{\text{batt}}} \int_0^t I_{\text{batt}}(SOC, P_{\text{batt}}, \theta)\, d\tau$. These two equations are then combined into (9.21).

It is equivalent in terms of energy to the *effective Ah-throughput*, Ah_{eff}, introduced in [14]. In the control problem this state is equivalent to Q_{loss}, in that it represents a measure of the degradation of the battery: any loss in capacity registered through an increase in Q_{loss} corresponds to an increase in E_{eff} of a commensurate magnitude.

Owing to the above definitions of the system states, the variables used in the control problem are rewritten as follows.

- Because SOC is a function of both E_{dep} (i.e., x_1) and Q_{batt} (or x_2), from (9.21), the battery current is also a function of the states x_1 and x_2:

$$I_{\text{batt}} = I_{\text{batt}}(SOC, P_{\text{batt}}, \theta) = I_{\text{batt}}(x_1, x_2, u, \theta) \tag{9.23}$$

- Similarly, the severity factor map is a function of both states:

$$\sigma_{\text{map}}(SOC, I_c, \theta) = \sigma_{\text{map}}\,(x_1, x_2, I_{\text{batt}}, \theta) \tag{9.24}$$

recalling that $I_c = I_{\text{batt}}/Q_{\text{batt}}$.

Thus, the state dynamics are as follows:

$$\dot{x}_1 = \dot{E}_{\text{dep}} = I_{\text{batt}}(x_1, x_2, u, \theta)\, V_{\text{oc,batt}}(x_1) \tag{9.25}$$

$$\dot{x}_2 = \dot{E}_{\text{eff}} = \sigma_{\text{map}}\,(x_1, x_2, I_{\text{batt}}, \theta)\ |I_{\text{batt}}(x_1, x_2, u, \theta)|\ V_{\text{oc,batt}}(x_1) \tag{9.26}$$

Finally, the following constraints are imposed to make the powertrain actuators operate within their physical limits (9.27a,9.27b,9.27c) and meet the total power request (9.27d):

$$0 \leq P_{\text{ice}} \leq P_{\text{ice,max}}(\omega_{\text{ice}}) \tag{9.27a}$$

$$P_{\text{em,min}}(\omega_{\text{em}}) \leq P_{\text{em}} \leq P_{\text{em,max}}(\omega_{\text{em}}) \tag{9.27b}$$

$$P_{\text{batt,min}} \leq P_{\text{batt}} \leq P_{\text{batt,max}} \tag{9.27c}$$

$$P_{\text{req}} = P_{\text{ice}} + P_{\text{em}} \tag{9.27d}$$

where $P_{\text{ice,max}}$ is the maximum engine power and it depends on ω_{ice} (in $[rpm]$); $P_{\text{em,min}}$ and $P_{\text{em,max}}$ are the minimum and maximum limits for the EM power, P_{em}, and they depend on the motor angular speed ω_{em} (in $[rpm]$); $P_{\text{batt,min}}$ and $P_{\text{batt,max}}$ are the constant minimum and maximum limits for the battery power. For the sake of simplicity, it is assumed that $P_{\text{em}} = P_{\text{batt}}$, which implies that the losses between the battery power output and the EM input are neglected.

Problem 1 (AL-EMP). The aging-limiting energy management problem (AL-EMP) consists in finding the optimal control sequence u^* which minimizes the cost function (9.18) under the dynamic constraints (9.25) and (9.26) and the global and local constraints (9.19) and (9.27).

In the standard energy management problem, battery aging is not accounted for and fuel consumption is the only cost being minimized; thus the constraint (9.19c) is not defined, as well as state (9.26) is not considered. The standard energy management problem is thus reduced to Problem 2.

Problem 2 (S-EMP). The standard energy management problem (S-EMP) consists in finding the optimal control sequence u^* which minimizes the cost function (9.18) under the dynamic constraint (9.25) and the global and local constraints (9.19a,9.19b) and (9.27).

9.6 Aging-Limiting Pontryagin's Minimum Principle Problem Solution

The Pontryagin's minimum principle (PMP) is used in this work to solve the AL-EMP. We refer to the solution of the AL-EMP through PMP as aging-limiting PMP (AL-PMP). To account for battery aging, an additional state (and, consequently, an additional costate) is added, as proposed in [16]. The Hamiltonian function for the AL-PMP is given by

$$H(u, P_{\text{req}}) = \dot{m}_f(u, P_{\text{req}})\, Q_{\text{lhv}} + \lambda_1 \dot{x}_1 + \lambda_2 \dot{x}_2 \tag{9.28}$$

where λ_1 is the first costate variable, relative to the depletion energy, and λ_2 is the second costate, relative to the effective energy-throughput; the state dynamics are defined in (9.25) and (9.26). If u^* is the optimal control input which minimizes (9.18) under the specified dynamic and global/local constraints, the following necessary conditions must hold true:

- u^* must minimize the Hamiltonian function H instantaneously;
- the governing equations of the optimal costates are given by

$$\begin{aligned} \dot{\lambda}_1^* &= -\frac{\partial H}{\partial x_1} \\ &= -\frac{\partial \dot{m}_f(u^*, P_{\text{req}})}{\partial x_1} Q_{\text{lhv}} - \lambda_1^* \frac{\partial \dot{x}_1}{\partial x_1} - \lambda_2^* \frac{\partial \dot{x}_2}{\partial x_1} \end{aligned} \tag{9.29}$$

$$\begin{aligned} \dot{\lambda}_2^* &= -\frac{\partial H}{\partial x_2} \\ &= -\frac{\partial \dot{m}_f(u^*, P_{\text{req}})}{\partial x_2} Q_{\text{lhv}} - \lambda_1^* \frac{\partial \dot{x}_1}{\partial x_2} - \lambda_2^* \frac{\partial \dot{x}_2}{\partial x_2} \end{aligned} \tag{9.30}$$

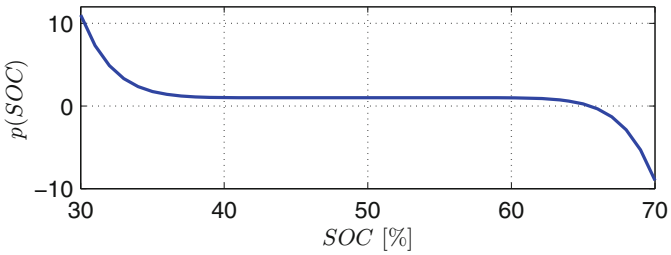

Fig. 9.12 Multiplicative penalty function for $SOC_{\text{ref}} = 50\,\%$, $SOC_{\text{min}} = 30\,\%$, $SOC_{\text{max}} = 70\,\%$, $a = 10$ and $b = 9$

The Hamiltonian (9.28) is modified by introducing a *penalty function*, $p(SOC)$, to limit the excursion of SOC during vehicle operation, thus enforcing the local state constraint (9.19b):

$$H(u, P_{\text{req}}) = \dot{m}_f(u, P_{\text{req}})\, Q_{\text{lhv}} + \lambda_1\, p(SOC)\, \dot{x}_1 + \lambda_2\, \dot{x}_2 \tag{9.31}$$

The penalty function on state of charge can be either additive or multiplicative, [1], and in this work the latter is chosen. Mathematically, a multiplicative penalty function is expressed as

$$p(SOC) = 1 - a \left(\frac{SOC - SOC_{\text{ref}}}{(SOC_{\text{min}} - SOC_{\text{max}})/2} \right)^b \tag{9.32}$$

This function acts modifying the cost of battery depletion in H according to the deviation of SOC from its target value SOC_{ref}. For positive a and odd b, $p = 1$ when $SOC = SOC_{\text{ref}}$; when $SOC < SOC_{\text{ref}}$, $p > 1$, resulting in an increase in the battery depleting cost in H; when $SOC > SOC_{\text{ref}}$, $p < 1$, thus decreasing the battery depleting cost in H. The penalty function, for the parameters values chosen in this work of $a = 10$ and $b = 9$, is shown in Fig. 9.12.

The choice of the initial costate values is referred to as *tuning* of the AL-PMP control strategy, and is discussed in Sect. 9.9.

Because $\dot{m}_f$ does not depend (at least in first approximation) on the second state, (9.29) and (9.30) can be expressed as

$$\dot{\lambda}_1^* = -\frac{\partial \dot{m}_f(P_{\text{batt}}, P_{\text{req}})}{\partial E_{\text{dep}}}\, Q_{\text{lhv}} - \lambda_1^* \frac{\partial \dot{E}_{\text{dep}}}{\partial E_{\text{dep}}} - \lambda_2^* \frac{\partial \dot{E}_{\text{eff}}}{\partial E_{\text{dep}}} \tag{9.33}$$

$$\dot{\lambda}_2^* = -\lambda_1^* \frac{\partial \dot{E}_{\text{dep}}}{\partial E_{\text{eff}}} - \lambda_2^* \frac{\partial \dot{E}_{\text{eff}}}{\partial E_{\text{eff}}} \tag{9.34}$$

The infinitesimal variation of E_{dep} upon an infinitesimal variation of SOC is obtained from (9.21). Thus, by means of using the following relations:

$$\begin{cases} \partial E_{\text{dep}} = -3600\, Q_{\text{batt}}\, V_{\text{oc,batt}}\, \partial SOC \\ \partial \dot{E}_{\text{dep}} = -3600\, Q_{\text{batt}}\, V_{\text{oc,batt}}\, \partial \dot{SOC} \end{cases} \tag{9.35}$$

the partial derivatives in (9.33) and (9.34) can be easily calculated from maps available in the powertrain model.

Thus (9.33) can be written as follows:

$$\begin{aligned} \dot{\lambda}_1^* = & \frac{\partial \dot{m}_f(P_{\text{batt}}, P_{\text{req}})}{\partial SOC} \frac{Q_{\text{lhv}}}{3600\, Q_{\text{batt}}\, V_{\text{oc,batt}}} - \lambda_1^* \frac{\partial \dot{SOC}}{\partial SOC} \\ & + \lambda_2^* \frac{\partial \dot{E}_{\text{eff}}}{\partial SOC} \frac{1}{3600\, Q_{\text{batt}}\, V_{\text{oc,batt}}} \end{aligned} \tag{9.36}$$

The term $\frac{\partial \dot{m}_f}{\partial SOC}$ is expressed as

$$\frac{\partial \dot{m}_f(P_{\text{batt}}, P_{\text{req}})}{\partial SOC} = \frac{\partial \dot{m}_f(P_{\text{batt}}, P_{\text{req}})}{\partial P_{\text{batt}}} \frac{\partial P_{\text{batt}}(SOC)}{\partial SOC} \tag{9.37}$$

where the first contribution is computed as

$$\frac{\partial \dot{m}_f(P_{\text{batt}}, P_{\text{req}})}{\partial P_{\text{batt}}} = -\frac{\partial \dot{m}_f(P_{\text{ice}}, P_{\text{req}})}{\partial P_{\text{ice}}} \tag{9.38}$$

since $P_{\text{batt}} = P_{\text{req}} - P_{\text{ice}}$. The term $\frac{\partial \dot{m}_f}{\partial P_{\text{ice}}}$ is the engine map, used in the vehicle simulator. The term $\frac{\partial \dot{m}_f}{\partial P_{\text{batt}}}$, on the other hand, is shown in Fig. 9.13.

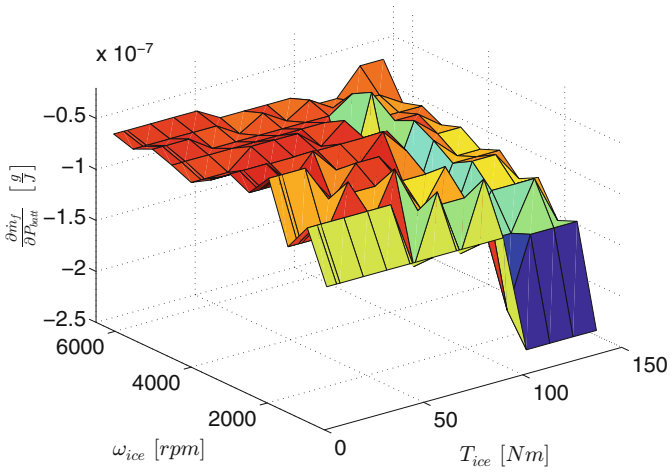

Fig. 9.13 Map depicting $\frac{\partial \dot{m}_f}{\partial P_{\text{batt}}}$ on the T_{ice}–ω_{ice} plane

From (9.14):

$$\frac{\partial P_{\text{batt}}(SOC)}{\partial SOC} = N_s N_p \frac{\partial P_{\text{cell}}(SOC)}{\partial SOC} \tag{9.39}$$

where $\frac{\partial P_{\text{cell}}}{\partial SOC}$ is available from the battery model. The resulting $\frac{\partial P_{\text{batt}}}{\partial SOC}$ map is shown in Fig. 9.14.
The term $\frac{\partial \dot{SOC}}{\partial SOC}$ is also extracted from the battery model and is shown in Fig. 9.15.

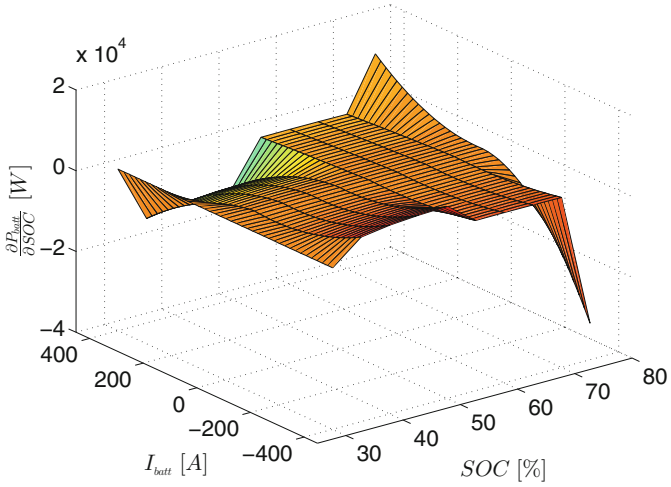

Fig. 9.14 Map depicting $\frac{\partial P_{\text{batt}}}{\partial SOC}$ on the SOC–I_{batt} plane

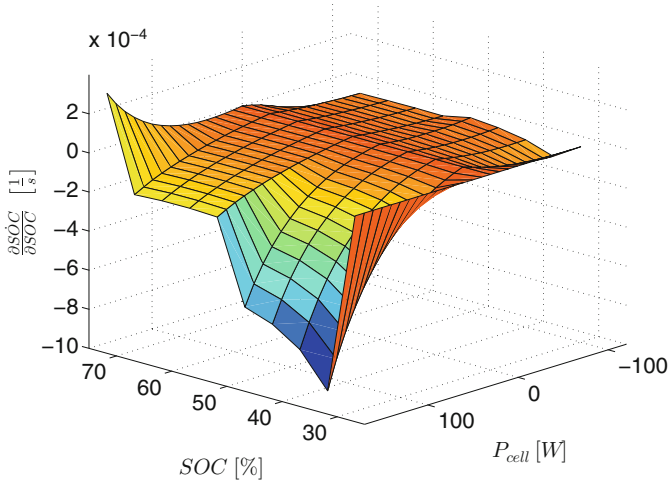

Fig. 9.15 Map depicting $\frac{\partial \dot{SOC}}{\partial SOC}$ on the P_{cell}-SOC plane

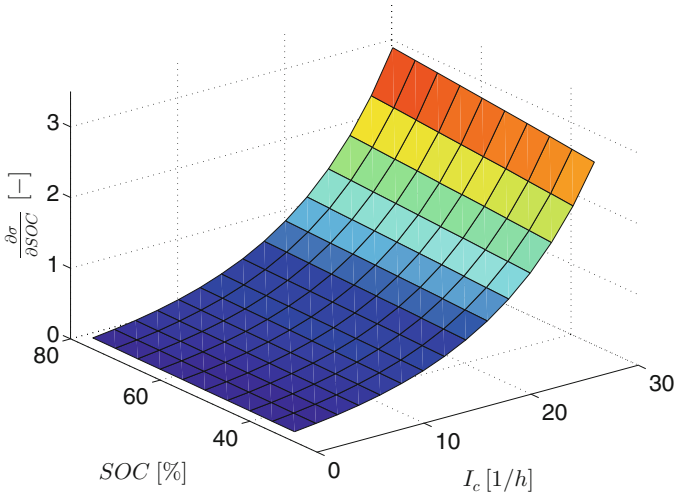

Fig. 9.16 Map depicting $\frac{\partial \sigma_{\text{map}}}{\partial SOC}$ on the I_c–SOC plane, for $\theta = 30°\text{C}$

Finally, $\frac{\partial \dot{E}_{\text{eff}}}{\partial SOC}$ is computed from (9.26) as

$$\begin{aligned}\frac{\partial \dot{E}_{\text{eff}}}{\partial SOC} =& \frac{\partial \sigma_{\text{map}}\left(E_{\text{dep}}, E_{\text{eff}}, I_{\text{batt}}, \theta\right)}{\partial SOC} \\ & \cdot \left|I_{\text{batt}}(E_{\text{dep}}, E_{\text{eff}}, P_{\text{batt}}, \theta)\right| V_{\text{oc,batt}} \\ & + \frac{\partial \left|I_{\text{batt}}(E_{\text{dep}}, E_{\text{eff}}, P_{\text{batt}}, \theta)\right|}{\partial SOC} \\ & \cdot \sigma_{\text{map}}\left(E_{\text{dep}}, E_{\text{eff}}, I_{\text{batt}}, \theta\right)\ V_{\text{oc,batt}}\end{aligned} \tag{9.40}$$

where the terms $\frac{\partial \sigma_{\text{map}}}{\partial SOC}$ and $\frac{\partial |I_{\text{batt}}|}{\partial SOC}$ are shown in Figs. 9.16 and 9.17, respectively.

The dynamics of the first costate can be numerically computed from the maps just shown.

The second costate dynamics, (9.34), can be written (from (9.25) and (9.26)) as

$$\begin{aligned}\dot{\lambda}_2^* =& -\lambda_1^* \frac{\partial I_{\text{batt}}(E_{\text{dep}}, E_{\text{eff}}, P_{\text{batt}}, \theta)}{\partial E_{\text{eff}}} V_{\text{oc,batt}}(E_{\text{dep}}) \\ & -\lambda_2^* \frac{\partial \left[\sigma_{\text{map}}\left(E_{\text{dep}}, E_{\text{eff}}, I_{\text{batt}}, \theta\right)\ \left|I_{\text{batt}}(E_{\text{dep}}, E_{\text{eff}}, P_{\text{batt}}, \theta)\right|\right]}{\partial E_{\text{eff}}} \\ & \cdot V_{\text{oc,batt}}(E_{\text{dep}})\end{aligned} \tag{9.41}$$

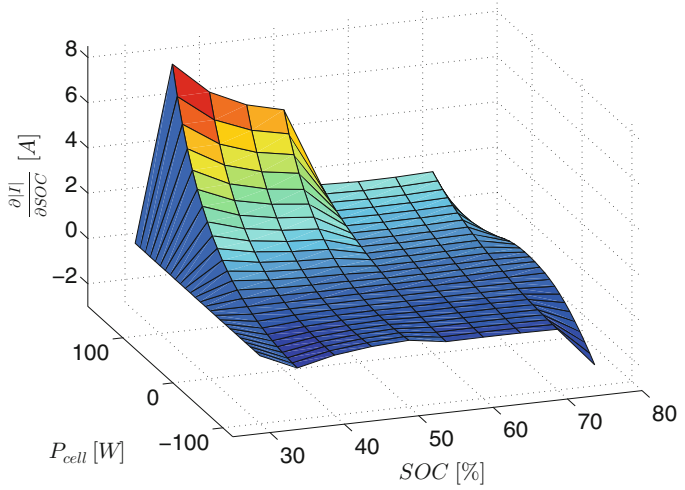

Fig. 9.17 Map depicting $\frac{\partial |I_{\text{batt}}|}{\partial SOC}$ on the SOC–P_{cell} plane

The partial derivatives in (9.41) are expressed as

$$\frac{\partial I_{\text{batt}}(E_{\text{dep}}, E_{\text{eff}}, P_{\text{batt}}, \theta)}{\partial E_{\text{eff}}} = \frac{\partial I_{\text{batt}}(SOC, P_{\text{batt}}, \theta)}{\partial SOC} \cdot \frac{\partial SOC(E_{\text{dep}}, E_{\text{eff}})}{\partial E_{\text{eff}}} \tag{9.42}$$

and

$$\begin{aligned} &\frac{\partial \left[\sigma_{\text{map}}(E_{\text{dep}}, E_{\text{eff}}, I_{\text{batt}}, \theta) \left|I_{\text{batt}}(E_{\text{dep}}, E_{\text{eff}}, P_{\text{batt}}, \theta)\right|\right]}{\partial E_{\text{eff}}} \\ &= \left[\frac{\partial \sigma_{\text{map}}(E_{\text{dep}}, E_{\text{eff}}, I_{\text{batt}}, \theta)}{\partial SOC} \left|I_{\text{batt}}(E_{\text{dep}}, E_{\text{eff}}, P_{\text{batt}}, \theta)\right| \right. \\ &\left. + \frac{\partial \left|I_{\text{batt}}(E_{\text{dep}}, E_{\text{eff}}, P_{\text{batt}}, \theta)\right|}{\partial SOC} \sigma_{\text{map}}(E_{\text{dep}}, E_{\text{eff}}, I_{\text{batt}}, \theta) \right] \\ &\cdot \frac{\partial SOC(E_{\text{dep}}, E_{\text{eff}})}{\partial E_{\text{eff}}} \end{aligned} \tag{9.43}$$

respectively. The term $\frac{\partial SOC}{\partial E_{\text{eff}}}$, appearing in both (9.42) and (9.43), was found to be negligible in simulation when compared to all the other costates dynamics terms (order of magnitude 10^{-8}), thus leading to the second costate dynamics to be approximated to $\dot{\lambda}_2^* \approx 0$, *i.e.* λ_2^* approximately constant:

$$\lambda_2^* \approx \lambda_{02}^* = const. \tag{9.44}$$

9.6.1 Comparison with Standard PMP Solution

The standard PMP solution is computed by minimizing the Hamiltonian function [1]:

$$H(u, P_{\text{req}}) = \dot{m}_f(u, P_{\text{req}})\, Q_{\text{lhv}} + \lambda\, \dot{x} \tag{9.45}$$

where the state x is the SOC, the costate is indicated with λ and its dynamics are

$$\dot{\lambda}^* = -\frac{\partial H}{\partial x} = -\lambda^* \frac{\partial \dot{x}}{\partial x} \tag{9.46}$$

When including battery aging consideration, the costate dynamics for the first state, as introduced in the present work, are

$$\dot{\lambda}^* = -\frac{\partial H}{\partial x} = \underbrace{-\frac{\partial \dot{m}_f(u^*, P_{\text{req}})}{\partial x} Q_{\text{lhv}}}_{\lambda_a} \underbrace{- \lambda^* \frac{\partial \dot{x}}{\partial x}}_{\lambda_b} \tag{9.47}$$

When comparing (9.46) and (9.47), one can see that the first term of (9.47), labeled as λ_a, is usually neglected in the standard PMP solution [14]. Simulation results (Fig. 9.18) show that this term gives a contribution to the costate dynamics which is of the same order of magnitude of the second term, labeled as λ_b. When the

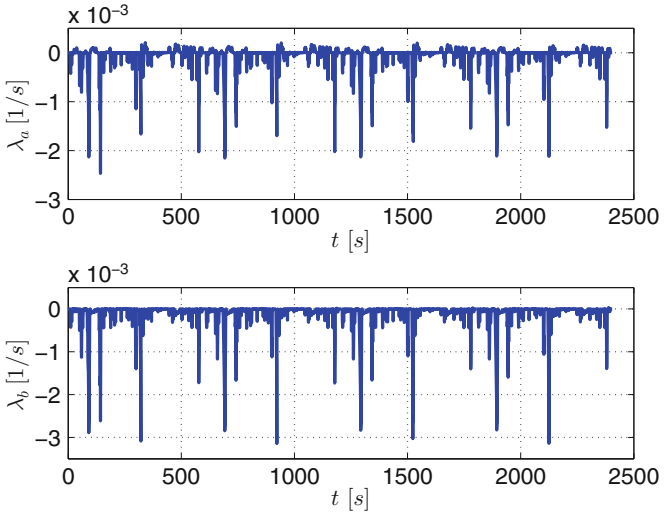

Fig. 9.18 Comparison of terms in $\dot{\lambda}^*$: $\lambda_a = -\frac{\partial \dot{m}_f}{\partial SOC} \frac{Q_{\text{lhv}}}{V_{\text{oc,batt}}\, Q_{\text{batt}}}$ (*top*) and $\lambda_b = -\lambda \frac{\partial \dot{SOC}}{\partial SOC}$ (*bottom*)

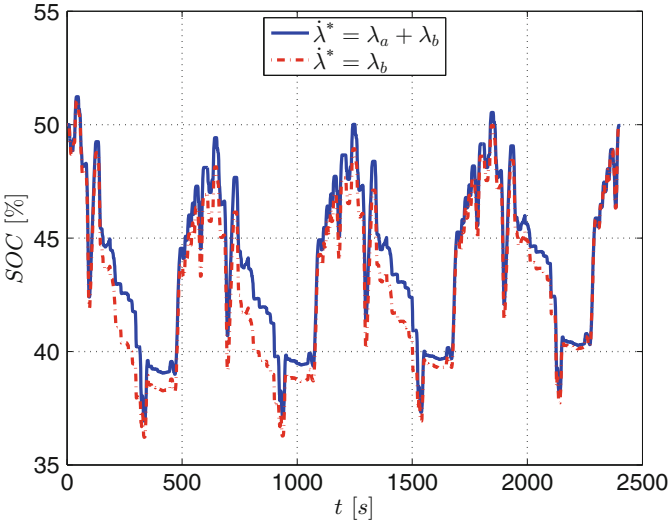

Fig. 9.19 Comparison of state of charge with and without the term $\lambda_a = -\frac{\partial \dot{m}_f}{\partial SOC} \frac{Q_{\text{lhv}}}{V_{\text{oc,batt}} Q_{\text{batt}}}$ in $\dot{\lambda}^*$

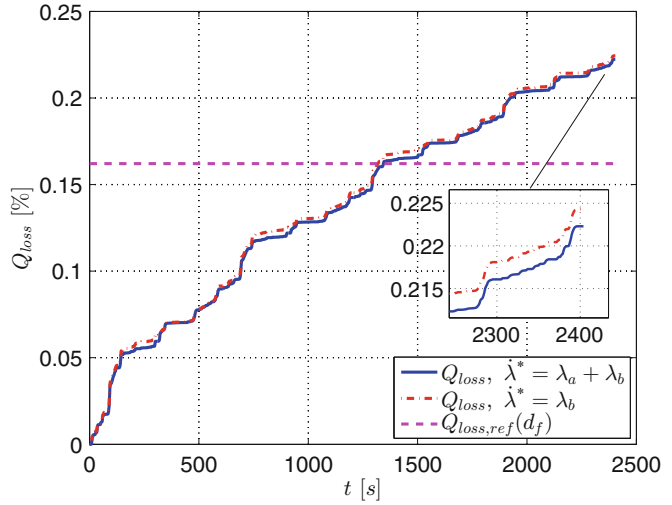

Fig. 9.20 Comparison of capacity loss with and without the term $\lambda_a = -\frac{\partial \dot{m}_f}{\partial SOC} \frac{Q_{\text{lhv}}}{V_{\text{oc,batt}} Q_{\text{batt}}}$ in $\dot{\lambda}^*$

term λ_a is kept in the overall solution, a slightly smaller *SOC* swing is observed, from Fig. 9.19, as well as a slight reduction of Q_{loss}, Fig. 9.20. The fuel economy is also slightly improved, 37.3206 *MPG* from 37.3048 *MPG* obtained when λ_a is not accounted for.

9.7 Remarks on Multi-Objective Optimal Control Formulation

In this section we show that the formulation of AL-PMP, as proposed in this paper, is equivalent to two other optimal control approaches, namely a multi-objective PMP and ECMS including aging consideration.

9.7.1 Multi-Objective PMP Problem

In this section, we show that the approach proposed in [14], i.e. a multi-objective optimal control formulation including fuel consumption and battery capacity degradation costs is equivalent to the method proposed in this paper. It is shown, though, that the AL-PMP gives some substantial advantages in terms of reduced tuning effort.

In [14] the cost function to be minimized is defined as the convex combination of two competing costs, i.e. fuel cost and aging cost, as follows:

$$J = \int_0^{t_f} (1-\alpha)\,\dot{m}_f + \frac{1}{3600}\,\alpha\,\frac{c_a}{\Gamma}\,\sigma_{\text{map}}\,|I_{\text{batt}}|\,dt \tag{9.48}$$

where α is a scalar parameter used to weight the two costs, c_a is a scalar, measured in $[g]$, which translates battery wear into equivalent fuel consumption, and $\Gamma = \frac{1}{3600}\int_0^{\text{EOL}} |I_{\text{batt,nom}}|\ dt$ is the total Ah-throughput under nominal cycling conditions. In [14], the dynamics of Ah_{eff} are given by

$$\dot{Ah}_{\text{eff}} = \frac{1}{3600}\,\sigma_{\text{map}}\,|I_{\text{batt}}| \tag{9.49}$$

and the Hamiltonian is written as

$$H = (1-\alpha)\,\dot{m}_f + \frac{1}{3600}\,\alpha\,\frac{c_a}{\Gamma}\,\sigma_{\text{map}}\,|I_{\text{batt}}| + \lambda\,\dot{SOC} \tag{9.50}$$

from which a PMP solution is computed, with dynamic constraints (9.7) and (9.49) and static constraints (9.19a, 9.19b) and optimal initial value of the costate λ_0^* found through the *shooting method*. The challenges with this formulation are that i) the choice of parameter value c_a is arbitrary and not necessarily trivial, and ii) a family of Pareto solutions is obtained as α is varied between 0 (only fuel consumption is considered in J) and 1 (only battery aging is considered in J), generating a trade-off between fuel and aging costs.

If we now normalize (9.50) (by $1-\alpha$ division and Q_{lhv} multiplication), we obtain

$$\begin{aligned}\bar{H} = \frac{Q_{\text{lhv}}}{1-\alpha} H =& \dot{m}_f\, Q_{\text{lhv}} + \frac{Q_{\text{lhv}}}{3600}\frac{\alpha}{1-\alpha}\frac{c_a}{\Gamma}\,\sigma_{\text{map}}\,|I_{\text{batt}}| \\ &+ Q_{\text{lhv}}\,\frac{\lambda}{1-\alpha}\left(-\frac{1}{3600\,Q_{\text{batt}}}\,I_{\text{batt}}\right)\end{aligned} \tag{9.51}$$

Defining $\bar{\lambda}_1 = Q_{\text{lhv}}\,\frac{\lambda}{\alpha-1}\,\frac{1}{3600\,Q_{\text{batt}}}$ and $\bar{\lambda}_2 = \frac{Q_{\text{lhv}}}{3600}\,\frac{\alpha}{1-\alpha}\,\frac{c_a}{\Gamma}$, the Hamiltonian is rewritten as

$$\bar{H} = \dot{m}_f\, Q_{\text{lhv}} + \bar{\lambda}_1\, I_{\text{batt}} + \bar{\lambda}_2\,\sigma_{\text{map}}\,|I_{\text{batt}}| \tag{9.52}$$

We can consider (9.52) as the Hamiltonian function associated with a control problem with a single objective cost function:

$$\bar{J} = \int_0^{t_f} \dot{m}_f\, dt \tag{9.53}$$

and the state dynamics given by (9.7), to account for battery depleting cost, with associate costate $\bar{\lambda}_1$, and (9.49) to account for battery aging with corresponding costate $\bar{\lambda}_2$.

Ultimately, the *two degrees of freedom* given by the choice of α and c_a are being translated into the costates $\bar{\lambda}_1$ and $\bar{\lambda}_2$.

The Hamiltonian of the AL-PMP solution, (9.28), can be written expressing explicitly the states dynamics as

$$H = \dot{m}_f\, Q_{\text{lhv}} + \lambda_1\, V_{\text{oc,batt}}\, I_{\text{batt}} + \lambda_2\, V_{\text{oc,batt}}\,\sigma_{\text{map}}\,|I_{\text{batt}}| \tag{9.54}$$

Comparing (9.54) and (9.52), one can clearly see the equivalence of the two problem formulations (same costs, (9.53) and (9.18), equivalent states, E_{dep} and E_{eff} and SOC and Ah_{eff}, respectively, as discussed in Sect. 9.5). In particular, the Hamiltonians (9.52) and (9.54) are identical under the conditions:

$$\begin{cases}\bar{\lambda}_1 = \lambda_1\, V_{\text{oc,batt}} \\ \bar{\lambda}_2 = \lambda_2\, V_{\text{oc,batt}}\end{cases} \tag{9.55}$$

or:

$$\begin{cases}\lambda_1 = \frac{Q_{\text{lhv}}}{3600\;Q_{\text{batt}}\,V_{\text{oc,batt}}}\,\frac{\lambda}{\alpha-1} \\ \lambda_2 = \frac{c_a\,Q_{\text{lhv}}}{3600\;\Gamma\,V_{\text{oc,batt}}}\,\frac{\alpha}{1-\alpha}\end{cases} \tag{9.56}$$

The advantages of using AL-PMP, though, is in that the challenge of selecting c_a and α is translated into optimally tuning the two costates λ_1, λ_2, which, in turn, boils down to solving Problem 1 with the AL-PMP algorithm presented in Sect. 9.9.

9.7.2 ECMS with Aging

In [26] it was shown that the PMP solution (of the S-EMP) is equivalent to the one given by ECMS. In this section, we want to show that a similar equivalence exists in the case of aging inclusion.

Under system dynamics:

$$\dot{E}_{\text{batt}} = I_{\text{batt}}(x_1, x_2, u, \theta)\, V_{\text{batt}}(x_1) \tag{9.57}$$

$$\dot{E}_{\text{eff}} = \sigma_{\text{map}}\,(x_1, x_2, I_{\text{batt}}, \theta)\;\; |I_{\text{batt}}(x_1, x_2, u, \theta)|\;\; V_{\text{oc,batt}}(x_1) \tag{9.58}$$

we want to instantaneously minimize the *equivalent fuel power*, $P_{f,\text{eqv}}$, given by the sum of the actual fuel power, P_f, and P_{dep} and P_{agn}:

$$P_{f,\text{eqv}} = P_f + P_{\text{dep}} + P_{\text{agn}} \tag{9.59}$$

where P_{dep} is the virtual fuel power associated with battery depletion and P_{agn} is the virtual fuel power associated with battery aging.

In particular, P_{dep} is defined as follows:

$$P_{\text{dep}} = s_1\, \dot{E}_{\text{batt}} \tag{9.60}$$

where s_1 is the *equivalency factor* which translates the battery depletion power into equivalent fuel power.

Usually, a value for s_1 when the battery is being charged, $s_{1,\text{chg}}$, and one when the battery is being discharged, $s_{1,\text{dis}}$ are used.

P_{agn} is defined as follows:

$$P_{\text{agn}} = s_2\, \dot{E}_{\text{eff}} \tag{9.61}$$

where s_2 is the equivalency factor associated with the battery aging power. This term introduces an additional equivalent fuel power when the battery is irreversibly aged.

Substituting equations (9.60) and (9.61) into the equivalent fuel power (9.59), yields to

$$P_{f,\text{eqv}} = \dot{m}_f\, Q_{\text{lhv}} + s_1\, V_{\text{batt}}\, I_{\text{batt}} + s_2\;\, V_{\text{oc,batt}}\, \sigma_{\text{map}}\, |I_{\text{batt}}| \tag{9.62}$$

The relation between the battery open circuit voltage and terminal voltage is by means of battery efficiency η_{batt}:

$$V_{\text{batt}} = \begin{cases} \eta_{\text{batt}} V_{\text{oc,batt}} & \text{if } I_{\text{batt}} \geq 0 \\ \frac{1}{\eta_{\text{batt}}} V_{\text{oc,batt}} & \text{if } I_{\text{batt}} < 0 \end{cases} \tag{9.63}$$

Defining:

$$\bar{s}_1 = \begin{cases} \bar{s}_{1,\text{dis}} = s_{1,\text{dis}}\, \eta_{\text{batt}} & \text{if } I_{\text{batt}} \geq 0 \\ \bar{s}_{1,\text{chg}} = \frac{s_{1,\text{chg}}}{\eta_{\text{batt}}} & \text{if } I_{\text{batt}} < 0 \end{cases} \tag{9.64}$$

(9.62) is written as follows:

$$P_{f,\text{eqv}} = \dot{m}_f\, Q_{\text{lhv}} + \bar{s}_1\, V_{\text{oc,batt}}\, I_{\text{batt}} + s_2\, V_{\text{oc,batt}}\, \sigma_{\text{map}}\, |I_{\text{batt}}| \tag{9.65}$$

which simply shows that ECMS with aging consideration and AL-PMP are equivalent. In addition,

$$\begin{cases} \lambda_1 = \bar{s}_1 \\ \lambda_2 = s_2 \end{cases} \tag{9.66}$$

hence:

$$s_1 = \begin{cases} \frac{\lambda_1}{\eta_{\text{batt}}} & \text{if } I_{\text{batt}} \geq 0 \\ \lambda_1\, \eta_{\text{batt}} & \text{if } I_{\text{batt}} < 0 \end{cases} \tag{9.67}$$

9.8 Penalty Function on Capacity Loss

A penalty function on capacity loss, $q(Q_{\text{loss}}, d)$, is introduced in the AL-PMP formulation to guarantee the targeted loss of capacity over each single day of driving. The Hamiltonian (9.31) becomes as follows:

$$H(u, P_{\text{req}}) = \dot{m}_f(u, P_{\text{req}})\, Q_{\text{lhv}} + \lambda_1\, p(SOC)\, \dot{x}_1 + \lambda_2\, q(Q_{\text{loss}}, d)\, \dot{x}_2 \tag{9.68}$$

where $p(SOC)$ enforces the local constraint on the state of charge. Contrary to the state of charge, for which positive and negative variations are allowed, the capacity loss (or effective energy-throughput) is a monotonically increasing function. To account for this characteristic, the proposed penalty function, $q(Q_{\text{loss}}, d)$, is a function of the driven distance.

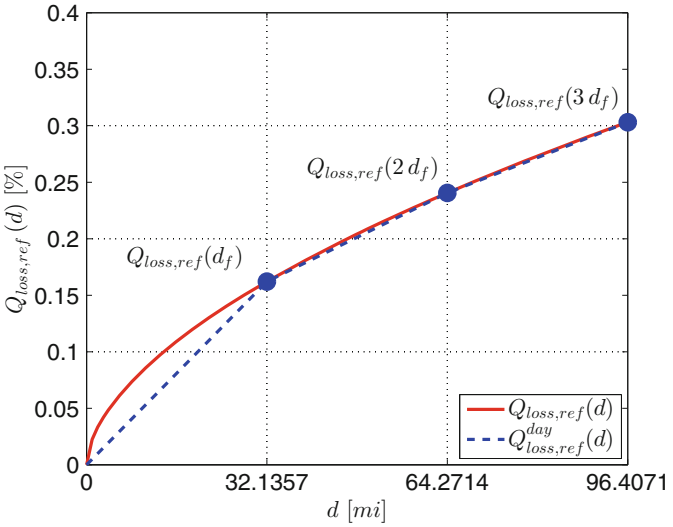

Fig. 9.21 $Q_{\text{loss,ref}}(d)$, $Q^{\text{day}}_{\text{loss,ref}}(d)$, and $Q_{\text{loss,ref}}(kd_f)$ over the first three days of US06 driving cycles, with $d_f = 32.1357mi$

We indicate as $Q^{\text{day}}_{\text{loss,ref}}(d)$ the reference capacity loss trajectory on a given day, d, with $d \in \left[(k-1)d_f,\, kd_f\right]$, in between the capacity loss of the previous day, $Q_{\text{loss,ref}}((k-1)d_f)$, and the following day $Q_{\text{loss,ref}}(kd_f)$:

$$Q^{\text{day}}_{\text{loss,ref}}(d) = \frac{Q_{\text{loss,ref}}(kd_f) - Q_{\text{loss,ref}}((k-1)d_f)}{d_f} \cdot d \tag{9.69}$$

In Fig. 9.21, $Q^{\text{day}}_{\text{loss,ref}}(d)$ is shown along with $Q_{\text{loss,ref}}(d)$ for the case of three days of US06 driving.

The linear reference $Q^{\text{day}}_{\text{loss,ref}}$ represents the maximum achievable capacity loss trajectory over one day of driving and its purpose is to *control* fast capacity loss at the beginning of each the driving day.

For implementation reasons, we define the maximum daily capacity loss to be equal to the daily reference loss plus a tolerance value (in the positive direction only, indicated as $Q^{+}_{\text{loss,tol}}$; this is assumed of the same value as the one used in Sect. 9.9 for the tolerance on ΔQ_{loss}, *i.e.* final state deviation from the daily target, namely $= 0.00324\,\%$):

$$Q_{\text{loss,max}}(d) = Q^{\text{day}}_{\text{loss,ref}}(d) + Q^{+}_{\text{loss,tol}} \tag{9.70}$$

The penalty function assumes then the following expression:

$$\begin{cases} q(Q_{\text{loss}}, d) = 1 + g \left(\frac{Q_{\text{loss}} - Q^{\text{day}}_{\text{loss,ref}}(d)}{Q^{+}_{\text{loss,tol}}} \right)^{h} \\ \qquad \text{for } Q^{\text{day}}_{\text{loss,ref}}(d) < Q_{\text{loss}} \leq Q_{\text{loss,max}}(d) \\ q(Q_{\text{loss}}, d) = 1 \qquad \text{for } Q_{\text{loss}} \leq Q^{\text{day}}_{\text{loss,ref}}(d) \end{cases} \tag{9.71}$$

It is worth noting that the $q(Q_{\text{loss}}, d)$ function is asymmetrical with respect to Q_{loss}. The parameter g is the gain of the penalty function, and increasing its value will result in an increase of the overall function value, as shown in Fig. 9.22; the parameter h is the exponent of the penalty function, and its effect is to change the function shape, as shown in Fig. 9.23. The ultimate effect of this change in shape is in a delayed intervention of the function (as h increases) on the aging cost in the instantaneous optimization. For large values of h the aging is weighted more and more only for large values of $Q_{\text{loss}} - Q^{\text{day}}_{\text{loss,ref}}(d)$, whereas smaller values of h are used when a more conservative approach on the aging is needed. In Fig. 9.24 the three-dimensional shape of the penalty function on capacity loss is presented when driven distance is included as well.

In the following section, the tuning of AL-PMP is presented, which, ultimately, consists in finding the optimal pair of initial values for the two costates $(\lambda^{*}_{01}, \lambda^{*}_{02})$.

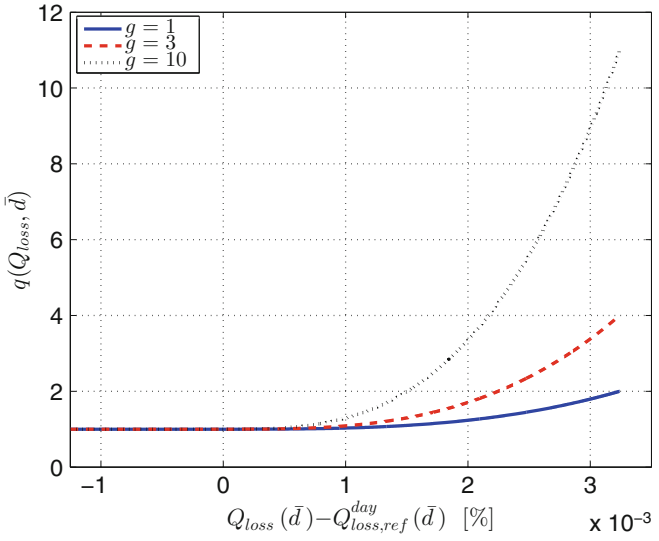

Fig. 9.22 Shape of the penalty function on Q_{loss} for different values of g and for a fixed value of $d = \bar{d}$. Negative values on the abscissa indicate that the battery can age less than its target daily value

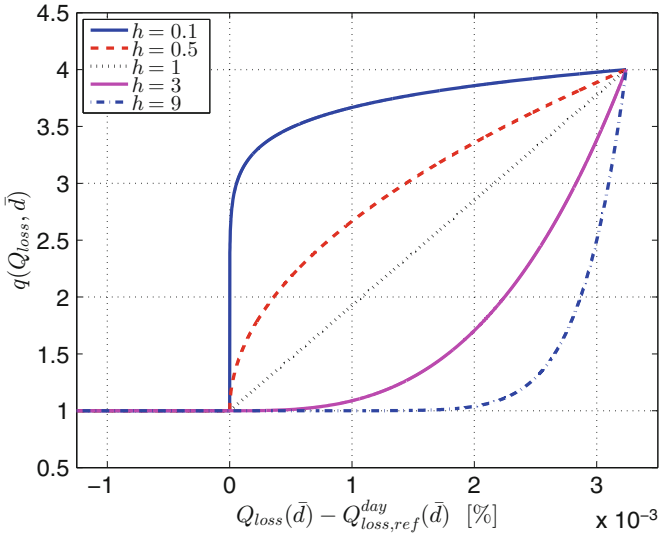

Fig. 9.23 Shape of the penalty function on Q_{loss} for different values of h, for a fixed value of $d = \bar{d}$

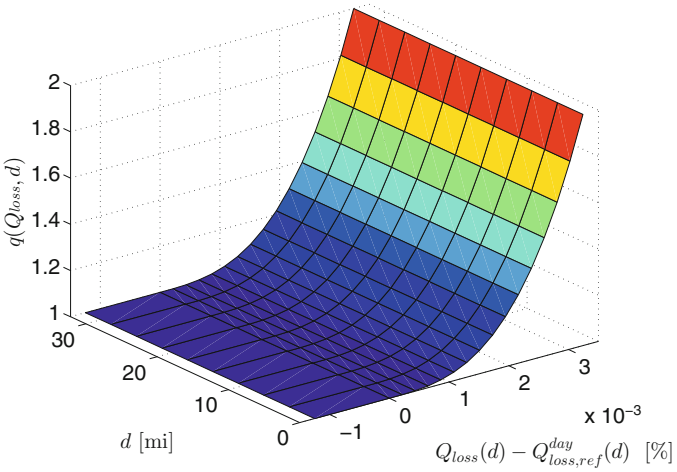

Fig. 9.24 Shape of the penalty function $q(Q_{\text{loss},d})$, as a function of Q_{loss} and d, with $g = 1$ and $h = 3$

9.9 AL-PMP Solution via Map-Based Tuning

In this section, the problem of finding the optimal pair of values $(\lambda_{01}^*, \lambda_{02}^*)$ in the AL-PMP strategy, that gives minimum fuel consumption m_f in $[kg]$ over the first day of driving with both state of charge and capacity loss regulated to their target values, is solved.

In the standard PMP solution, *shooting method* is used to iteratively tune λ_0 in order to obtain charge-sustainability [5]. This is possible given the bijective relationship between λ_0 and $SOC(d_f)$. In the AL-PMP the two costate dynamics are highly non-linear and coupled with no clear relation among them. For this reason, a new approach is proposed to tune the optimal supervisory controller.

An initial guess value for both costates is defined through the set Λ_0:

$$\Lambda_0 = \{(\lambda_{01}, \lambda_{02}) \mid \lambda_{01} \in \Lambda_{01}, \lambda_{02} \in \Lambda_{02}\} \tag{9.72}$$

where the vectors Λ_{01} and Λ_{02} are given by

$$\begin{aligned} \Lambda_{01} &= [\lambda_{01,\min} : \lambda_{01,\text{incr}} : \lambda_{01,\max}] \\ \Lambda_{02} &= [\lambda_{02,\min} : \lambda_{02,\text{incr}} : \lambda_{02,\max}] \end{aligned} \tag{9.73}$$

where the subscripts *max* and *min* are the maximum and minimum value for each costate and the subscript *incr* stands for the increment selected for the costates within that interval. Starting from each pair of initial values within the set Λ_0 AL-PMP is solved (state and costate dynamics are integrated forward in time) and three values are stored, namely:

- m_f,
- $\Delta SOC = SOC(d_f) - SOC_{\text{ref}}$,
- $\Delta Q_{\text{loss}} = Q_{\text{loss}}(d_f) - Q_{\text{loss,ref}}(d_f)$,

where ΔSOC and ΔQ_{loss} are the deviation of SOC and Q_{loss} from their target values at the end of the driving horizon, SOC_{ref} for the state of charge and $Q_{\text{loss,ref}}(d_f)$ for the capacity loss, respectively. Three matrices are built registering those final values for each pair of initial costates. These *maps* are easily plotted as function of λ_{01} and λ_{02}. From the generation of the three maps the optimal pair of costate is found as

$$(\lambda_{01}^*, \lambda_{02}^*) = \{(\lambda_{01}, \lambda_{02}) \mid \Delta SOC = 0 \wedge \Delta Q_{\text{loss}} = 0\} \tag{9.74}$$

The numerical value is found by means of the tuning algorithm presented next.

9.9.1 Tuning Algorithm Flowchart

The tuning procedure, summarized in the flowchart of Fig. 9.25, is composed of the following steps.[3]

[3] An important aspect of the tuning algorithm concerns the tolerances on the final state values. The approach followed in this work is as follows. Regarding SOC, a tolerance interval $SOC_{\text{tol}} = \pm 1\,\%$ is accepted for the charge-sustainability target. This means that all the values $\Delta SOC \in [-1, 1]\%$ are considered within the tolerance, and as such they are defined *sub-optimal* values. The *optimal* value is only one, i.e. $\Delta SOC^* = 0$, and it falls inside the tolerance interval. For Q_{loss} a similar

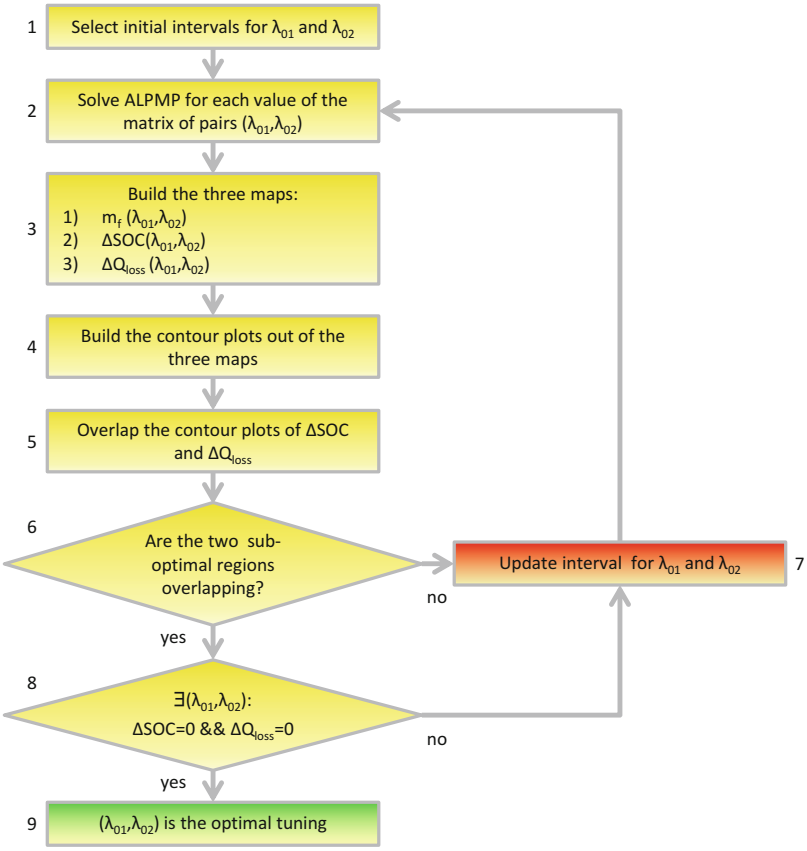

Fig. 9.25 AL-PMP tuning algorithm flowchart

1. The initial intervals for λ_{01} and λ_{02} are selected, thus vectors Λ_{01} and Λ_{02} and set Λ_0 are defined.
2. For each point of the set Λ_0, *i.e.* pairs $(\lambda_{01}, \lambda_{02})$, Problem 1 is solved.
3. m_f, ΔSOC, and ΔQ_{loss} are stored for each pair in Λ_0 and the corresponding maps are built.
4. The iso-value curves are plotted from the maps obtained in Step 3.
5. The contour plots of ΔSOC and ΔQ_{loss} intersect.

relative tolerance is considered and computed as follows. Given an $SOC_{\text{tol}} = \pm 1\,\%$ and a state of charge target of $SOC_{\text{ref}} = 50\,\%$, the relative tolerance for SOC is given by $SOC^{\text{rel}}_{\text{tol}} = \frac{\pm 1[\%]}{50\,\%}\,100 = \pm 2\,\%$; the relative tolerance for Q_{loss} is then $Q^{\text{rel}}_{\text{loss,tol}} = SOC^{\text{rel}}_{\text{tol}} = \pm 2\,\%$. The target for capacity loss, as explained in Sect. 9.2.1, for 4 US06 driving cycles ($d_f = 32.14mi$) is $Q_{\text{loss,ref}}(d_f) = 0.16205\,\%$, which leads to $Q_{\text{loss,tol}} = \frac{0.16205\,\%}{100}\,(\pm 2\,\%) = \pm 0.00324\,\%$. The *sub-optimal* values of capacity loss deviation are $\Delta Q_{\text{loss}} \in [-0.00324, 0.00324]\%$ and the *optimal* value is $\Delta Q^*_{\text{loss}} = 0$.

6. If the sets where both $SOC(d_f)$ and $Q_{\text{loss}}(d_f)$ are within the tolerance, i.e. $\Delta SOC \in SOC_{\text{tol}}$ and $\Delta Q_{\text{loss}} \in Q_{\text{loss,tol}}$ exists, go to Step 8, otherwise go to Step 7.
7. The solution is not found within the originally defined initial guess values for the costates, and the vectors Λ_{01} and Λ_{02} are updated.
8. The subset of Λ_0 for which both $SOC(d_f)$ and $Q_{\text{loss}}(d_f)$ lie on their respective target value, i.e. $\Delta SOC = 0$ and $\Delta Q_{\text{loss}} = 0$, is found.
9. The point $(\lambda_{01}^*, \lambda_{02}^*)$ in the set Λ_0 such that Step 8 is verified is the optimal tuning.

9.10 Simulation Results

Simulation results are shown in this section that implements the algorithm of Fig. 9.25. Four US06 driving cycles are simulated at an external temperature $\theta_{\text{amb}} = 30°\text{C}$, where it is imposed $SOC_{\text{ref}} = 50\,\%$, $SOC_{\text{min}} = 30\,\%$ and $SOC_{\text{max}} = 70\,\%$.

First, the initial intervals for the costates, as defined in (9.73), are chosen (Step 1):

$$\begin{aligned} \Lambda_{01} &= [2.00 : 0.04 : 2.60] \\ \Lambda_{02} &= [0.080 : 0.004 : 0.140] \end{aligned} \tag{9.75}$$

Note that the values of the initial costates are in general different from each other, and that the resolutions are selected in order to have vectors of length not more than 20; in this way Λ_0 contains not more than 400 points and the simulations take around $2.5h$ as the most, on a machine with an Intel i7 quad-core processor @2GHz and 6GB RAM. If better accuracy is required, a narrower and finer interval can be defined around the optimal point. The AL-PMP is solved for each pair in Λ_0 (Step 2), and the output maps are obtained (Step 3) and depicted in Fig. 9.26.

The contour plots shown in Fig. 9.27 are obtained from the maps of Fig. 9.26 (Step 4). Next, the contour plots relative to ΔSOC and ΔQ_{loss} are intersected (Step 5) and their intersection is shown in the dark grey area of Fig. 9.28 (Step 6). Within the shaded region of Fig. 9.28, the optimal tuning (the magenta dot on the right-hand side of the figure) of AL-PMP is found (Step 8), and the optimal pair of initial costates (Step 9) is

$$\begin{cases} \lambda_{01}^* = 2.3257 \\ \lambda_{02}^* = 0.113 \end{cases} \tag{9.76}$$

When using the proposed tuning to execute the AL-PMP, the variation of the final states from their reference is found to be practically zero: $\Delta SOC = -0.036763\,\%$ and $\Delta Q_{\text{loss}} = -0.000046505\,\%$. When applying the standard PMP (nominally, solving Problem 2), a similar performance is obtained for SOC, as from Fig. 9.29,

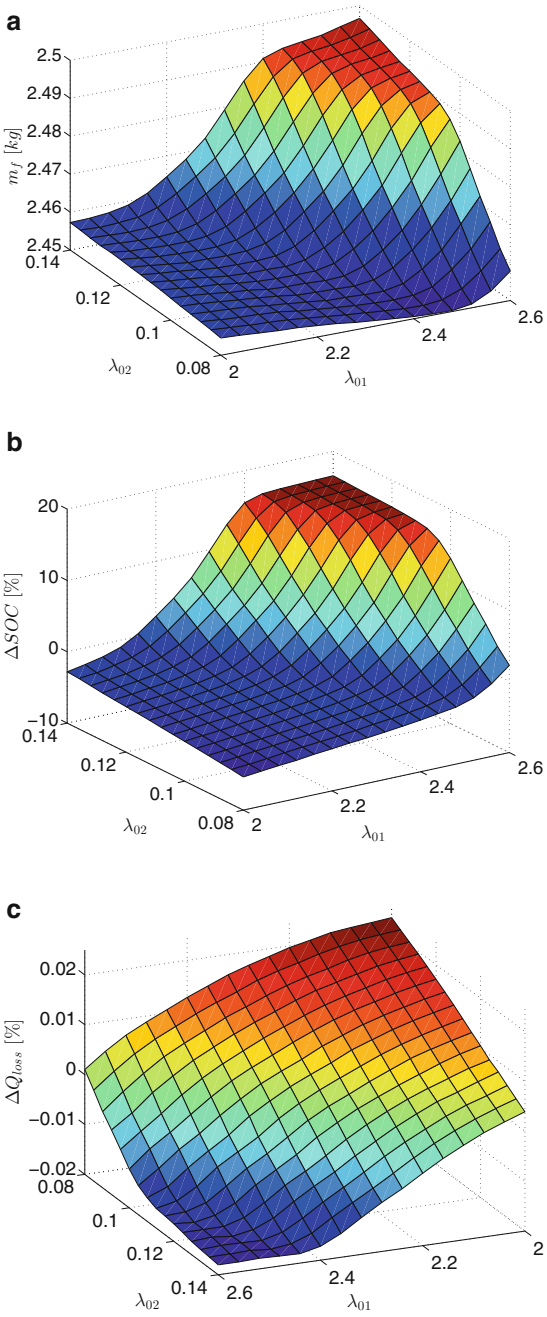

Fig. 9.26 Maps obtained for 4 US06 driving cycles at $\theta_{\text{amb}} = 30°\text{C}$, with the choice of initial costates from (9.75). (**a**) Fuel consumption. (**b**) Final state of charge variation with respect to target. (**c**) Final capacity loss variation with respect to target

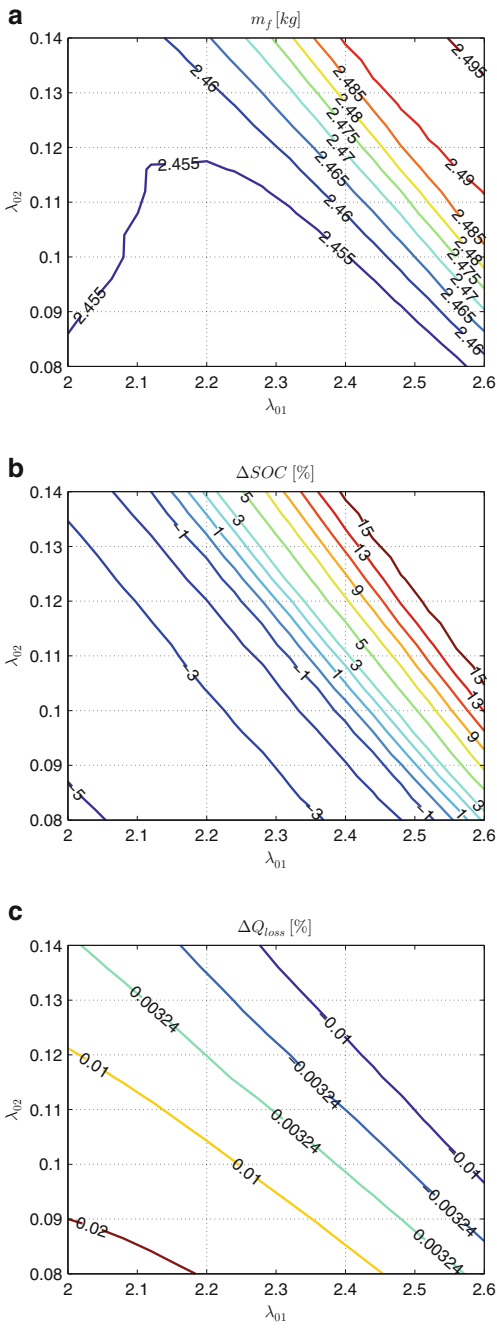

Fig. 9.27 Contour plots obtained for 4 US06 driving cycles at $\theta_{\text{amb}} = 30°\text{C}$, with the choice of initial costates as in (9.75). (**a**) Fuel consumption. (**b**) Final state of charge variation with respect to target. (**c**) Final capacity loss variation with respect to target

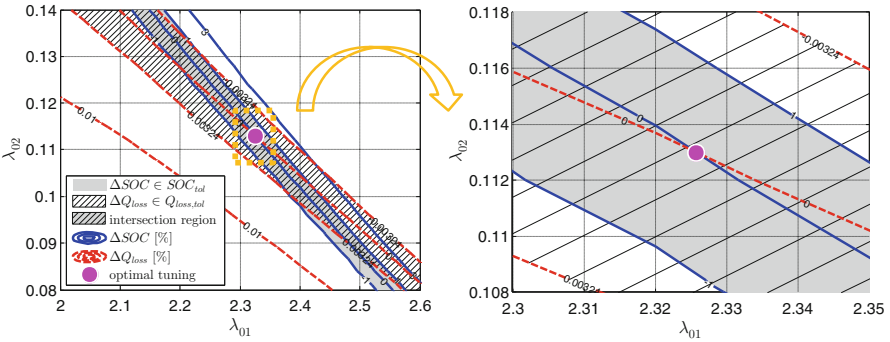

Fig. 9.28 Intersection of contour plots of Figs. 9.27b and c (*left plot*). The optimal solution (i.e.,, tuning) is found by the intersection of the 0-contour levels of ΔSOC and ΔQ_{loss} (as shown on the *right-hand side plot*)

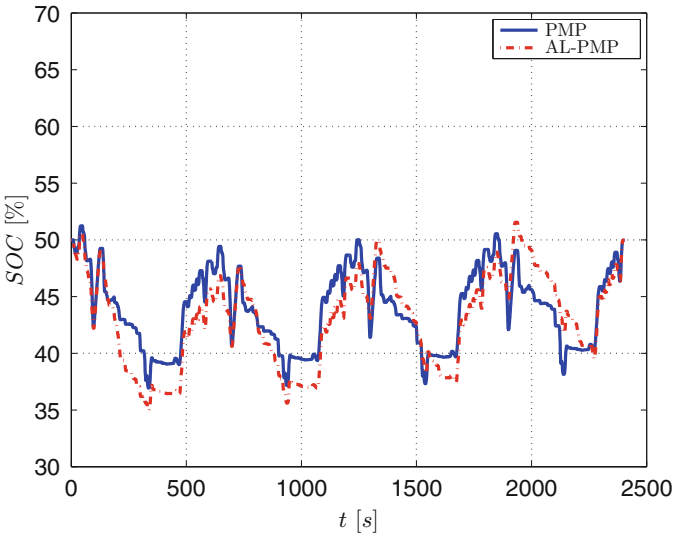

Fig. 9.29 Comparison of state of charge over the first day of driving for PMP and AL-PMP: both the strategies are able to regulate *SOC* to its reference value at the end of the day of driving

but Q_{loss} is not limited, as shown in Fig. 9.30: the capacity loss is more than 40 % higher than the target value (over the first day of driving). As a result, the target EOL will not be met, leading to a prematurely aged battery (when compared to vehicle life). From a fuel economy standpoint, on the other hand, only a slight difference is observed between PMP and AL-PMP, with just 0.56 % loss in terms of *MPG* for the latter (37.3206 for PMP and 37.1115 for AL-PMP).

Hence, significant reduction in battery aging at the price of a little worse fuel consumption is achieved when applying AL-PMP.

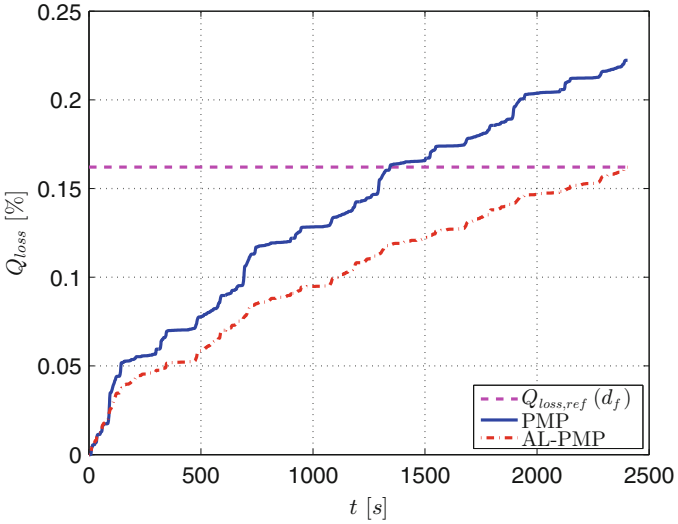

Fig. 9.30 Comparison of capacity loss over the first day of driving for PMP and AL-PMP: only AL-PMP is able to regulate Q_{loss} to its reference value at the end of the day of driving

Table 9.3 Comparison of optimal initial costate pairs $(\lambda_{01}^*, \lambda_{02}^*)$ in AL-PMP for different external temperatures over 4 US06 driving cycles

$\boldsymbol{\theta}_{\text{amb}}$ [°C]	$\boldsymbol{\lambda}_{01}^*$	$\boldsymbol{\lambda}_{02}^*$
20	3.1964	0.005954
25	3.0811	0.019333
29	2.565	0.082397
30	2.3257	0.113
31	1.8185	0.18396
32	1.0068	0.30417

In the following, AL-PMP solution is presented for different temperature scenarios.

9.10.1 Results for Different Ambient Temperatures

Simulation results are presented for different external ambient temperatures, over four US06 driving cycles. For each value of temperature considered, AL-PMP is tuned as described in Sect. 9.9. The optimal initial values of the costates are reported in Table 9.3 and shown in Fig. 9.31.

The optimal initial value of the first costate decreases with increasing temperature, while the optimal second costate is increasing. This can be explained thinking that higher temperatures represent more harmful conditions for the battery capacity loss. Given that, the aging term in the Hamiltonian (9.28), multiplied by λ_2, needs

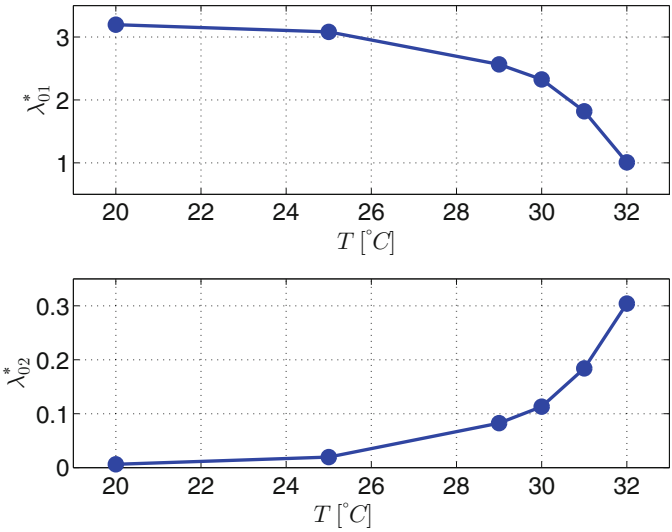

Fig. 9.31 Graphical representation of optimal initial costate values in AL-PMP for different external temperatures

to be weighted more in the optimization strategy than the fuel consumption and the battery charging/discharging term, the latter multiplied by λ_1.

The activation of the aging penalty function on capacity loss is not required when ambient temperature is below 33°C. For temperatures equal or above 33°C, the penalty function needs to be activated to obtain optimal capacity loss regulation, i.e. to find the optimal pair $(\lambda_{01}^*, \lambda_{02}^*)$ so that both ΔSOC and ΔQ_{loss} are exactly zero.

Nevertheless, simulation study shows that when the aging penalty function is *not* used in high temperature conditions, sub-optimal solutions are found. Namely, two ways are proposed to tune AL-PMP, which are presented in the following.

1. Tuning 1: optimal tuning is done for ΔSOC, and only sub-optimality is guaranteed for ΔQ_{loss}; this means that $\Delta SOC = 0$, while ΔQ_{loss} is chosen to be as close as possible to 0: the first condition selects the points on the plane that lie on the optimal *SOC* line, which is also within Q_{loss} tolerance.
2. Tuning 2: optimal tuning is done for ΔQ_{loss}, and only sub-optimality is guaranteed for ΔSOC; the points lie on the optimal Q_{loss} line, i.e. $\Delta Q_{\text{loss}} = 0$, and *SOC* is within the allowable tolerance.

The initial costate values found for the simulations performed are

1. Tuning 1:

$$\begin{cases} \lambda_{01} = 0.01 \\ \lambda_{02} = 0.4640 \end{cases} \tag{9.77}$$

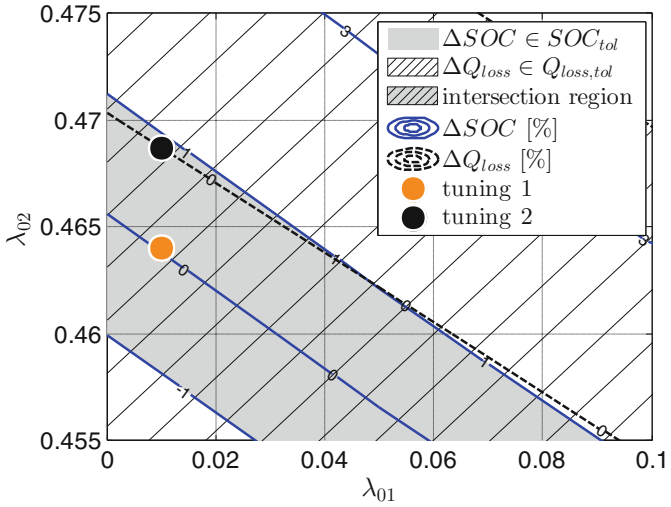

Fig. 9.32 Zoom on the intersection region of contour plots for 4 US06 driving cycles at $\theta_{\text{amb}} = 33°\text{C}$: the proposed tunings for AL-PMP are indicated with an orange spot (1—optimal for ΔSOC only) and a black spot (2—close-to-optimal for ΔQ_{loss} only)

Table 9.4 Results for the proposed tuning 1 and tuning 2 for $\theta_{\text{amb}} = 33°\text{C}$, in terms of relevant quantities: fuel consumption and final SOC and Q_{loss} deviations from targets

Tuning	m_f [kg]	ΔSOC [%]	ΔQ_{loss} [%]
1	2.4844	−0.031599	0.00084542
2	2.4862	0.87247	0.0000053273

2. Tuning 2:

$$\begin{cases} \lambda_{01} = 0.01 \\ \lambda_{02} = 0.4687 \end{cases} \tag{9.78}$$

as also shown in Fig. 9.32. Figures 9.33 and 9.34 show the results of the two tunings in terms of SOC and capacity loss profiles and Table 9.4 reports the numerical values of simulation outputs.

It is worth noting that the error on the target values for Q_{loss} in the tuning 1 and the error for SOC in the tuning 2 are very small. On the other hand, the capacity loss obtained from standard PMP is not even close to $Q_{\text{loss,ref}}(d_f)$: AL-PMP reduces Q_{loss} by more than 30 %, at the limited price of an increase of fuel consumption between 1.69 and 1.77 % ($m_f = 2.4430kg$ for PMP, see Table 9.4 for AL-PMP).

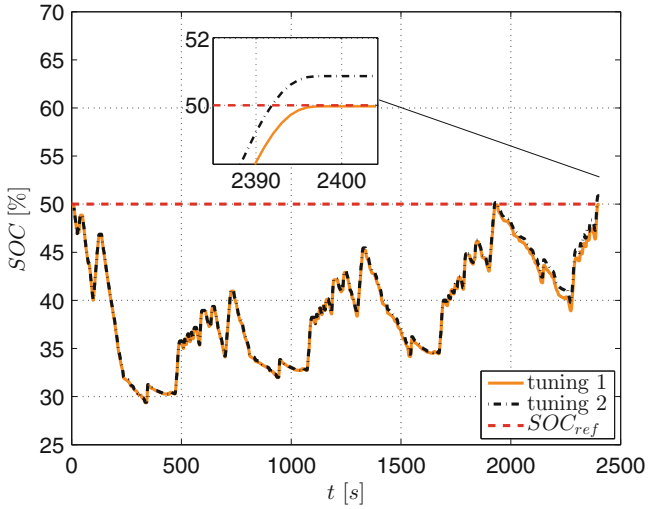

Fig. 9.33 State of charge profile for the proposed tuning 1 and tuning 2 for $\theta_{\text{amb}} = 33°\text{C}$. Note that *SOC* is below 30 % for a short time interval around $t = 300s$; this situation is penalized but allowed by the penalty function on *SOC*, which is a soft constraint in the optimization

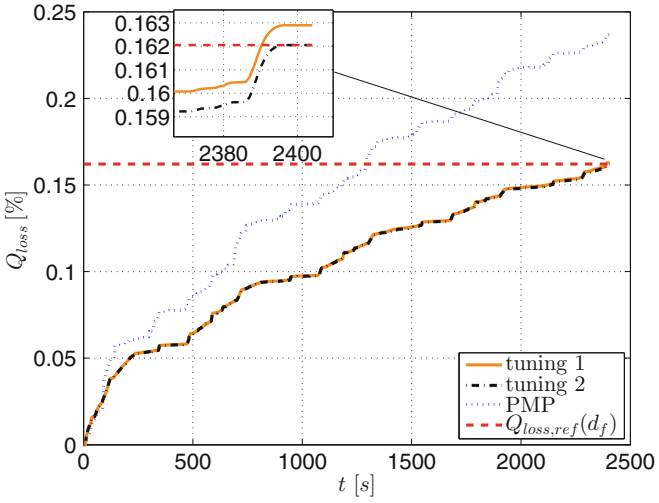

Fig. 9.34 Capacity loss profile for the proposed tuning 1 and tuning 2 for $\theta_{\text{amb}} = 33°\text{C}$. PMP solution is also reported

9.10.2 Results with Penalty Function

If the penalty function on aging dynamics is used, on the other hand, an optimal solution is found. From simulation results, at $\theta_{\text{amb}} = 33°\text{C}$, when using the

following calibration parameters for the aging penalty function:

$$\begin{cases} g = 3 \\ h = 1 \end{cases} \tag{9.79}$$

the optimal pair for the initial costate values is

$$\begin{cases} \lambda_{01}^{*} = 2.5859 \\ \lambda_{02}^{*} = 0.025833 \end{cases} \tag{9.80}$$

The resulting overlapped contour plots of ΔSOC and ΔQ_{loss} are shown in Fig. 9.35. In this case a well-defined intersection is obtained, hence the optimal solution is found.

Figure 9.36 shows the distribution of the operating points of the battery on the severity factor map contour plot, as a function of state of charge and C-rate, for a fixed battery temperature, both for PMP and AL-PMP. The distribution of points indicates that AL-PMP (b), compared to standard PMP (a), is effectively able to reduce the harshness of the battery operating conditions, since the maximum value reached in σ_{map} is less than 20 instead of almost 30, with lower C-rate of operation and larger state of charge range used. The engine efficiency map used by PMP and AL-PMP is shown in Fig. 9.37.

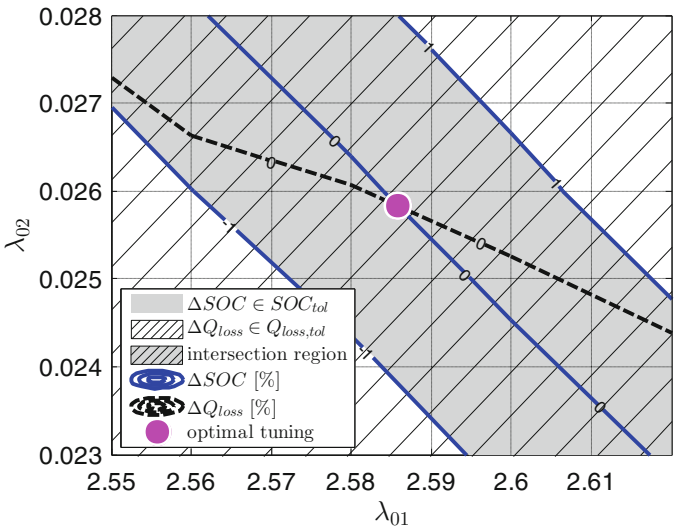

Fig. 9.35 Zoom on the intersection region of contour plots for 4 US06 driving cycles at $\theta_{\text{amb}} = 33°\text{C}$: the optimal tuning for AL-PMP with penalty function on Q_{loss} is indicated with a purple spot

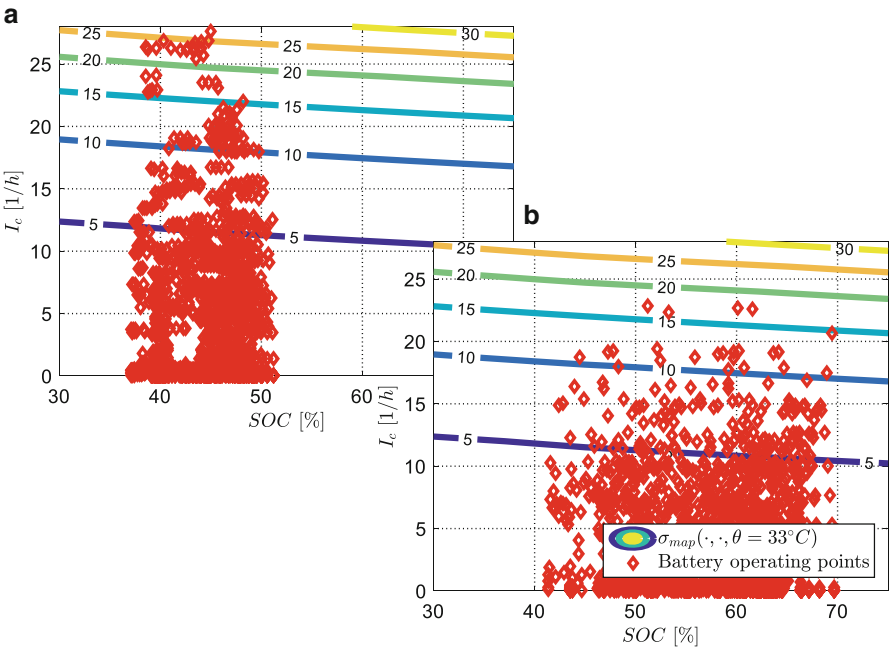

Fig. 9.36 Battery operating points on the severity factor map, for 4 US06 driving cycles at $\theta_{\text{amb}} = 33°\text{C}$: comparison between standard PMP (**a**) and AL-PMP (**b**)

Simulation results have shown that for extreme external temperatures combined with aggressive driving cycles like US06, AL-PMP cannot prevent the battery from aging more than the final daily target, even with the introduction of the penalty function. As an example, simulation results performed at $\theta_{\text{amb}} = 40°\text{C}$ and penalty function parameters

$$\begin{cases} g = 3 \\ h = 0.1 \end{cases} \tag{9.81}$$

are shown in Fig. 9.38 sub-optimal initial costates:

$$\begin{cases} \lambda_{01} = 0.1 \\ \lambda_{02} = 0.077 \end{cases} \tag{9.82}$$

One can see that both with or without penalty function, AL-PMP is not able to control capacity loss to its daily target. Nonetheless, the capacity loss is reduced by approximately 35 % from the PMP solution, and by about 7.5 % with respect to the AL-PMP solution without penalty function; furthermore, the final value of Q_{loss}, although not equal to $Q_{\text{loss,ref}}(d_f)$, is quite close to the target value.

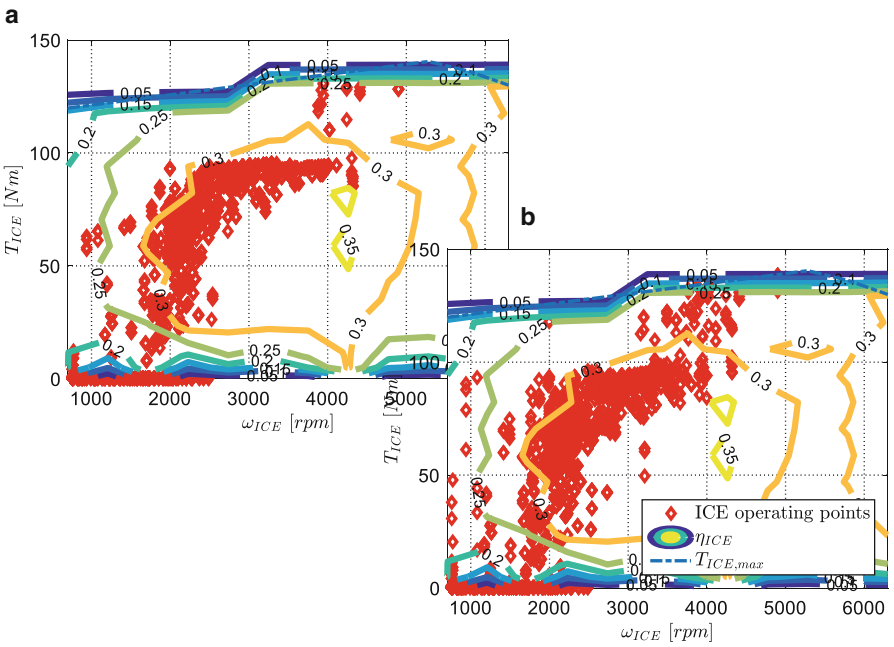

Fig. 9.37 Engine operating points for 4 US06 driving cycles at $\theta_{\text{amb}} = 33°\text{C}$: comparison between standard PMP (**a**) and AL-PMP (**b**)

Table 9.5 Simulation results for AL-PMP with penalty function ($g = 3, h = 0.1$) at $\theta_{\text{amb}} = 40°\text{C}$; comparison between discharge and charge phases

	Total	Discharge	Charge
Average I_c $[1/h]$	3.0257	1.9055	7.4036
Average θ [°C]	43.3322	43.2484	43.6600
Average σ_{map} $[-]$	4.5368	3.7351	7.6703
Extracted Ah	4.5472	2.2807	2.2665
Ah_{eff}	34.9286	10.1631	24.7655

In Table 9.5, discharge and charge battery events are compared for $\theta_{\text{amb}} = 40°\text{C}$. When using AL-PMP, only the discharge is being optimized. One can see that the C-rate in charge is on average almost four times larger than in discharge, with slightly higher temperature. Thus, on average the severity factor map is more than two times higher in charge, and so are the Ah_{eff}, which are directly related to aging, [14]. This means that the aging process takes place mostly during the charge phase (braking), which is not controlled with the present strategy. On the other hand, the extracted Ah are almost equal, as expected for a charge-sustaining HEV. This analysis emphasizes the importance to control battery charging, as also shown in Fig. 9.39, where the capacity loss profile is shown distinguishing between the discharge and charge phases. When Q_{loss} is controlled (discharge), it stays approximately constant, or increases at a small rate. When it is not controlled (charge), it undergoes important upwards steps that prevent to meet the daily target.

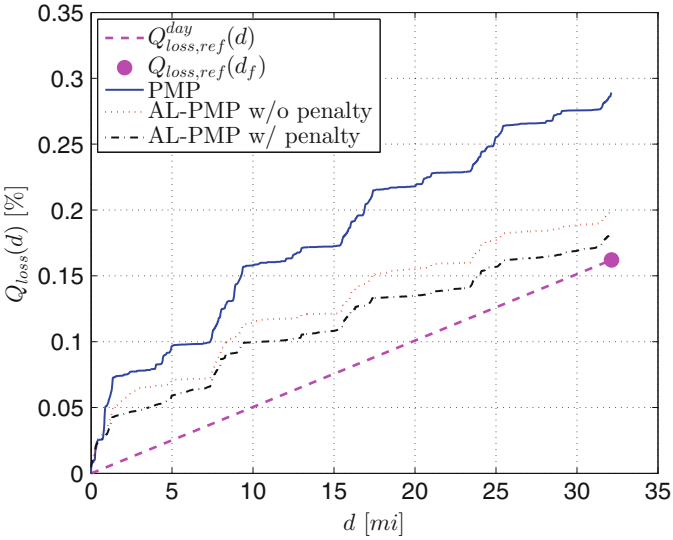

Fig. 9.38 Capacity loss results for $\theta_{\text{amb}} = 40°\text{C}$: comparison between PMP, AL-PMP with and without penalty function

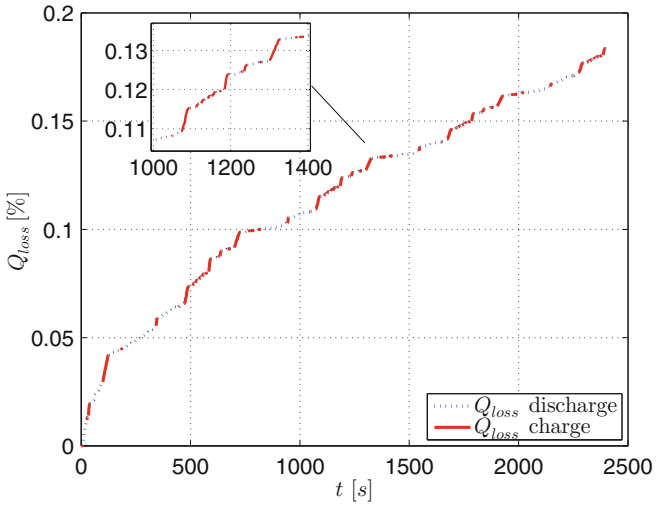

Fig. 9.39 Capacity loss profile for $\theta_{\text{amb}} = 40°\text{C}$ with the discharge and charge phases plotted separately

Simulations over a week of US06 driving (six days) are shown in Fig. 9.40, with $\theta_{\text{amb}} = 30°\text{C}$. The capacity loss reference values at the end of each day is tracked when using AL-PMP. Therefore, if battery degradation is not properly taken into account by the EMS, ultimately, the situation arises that an early replacement of

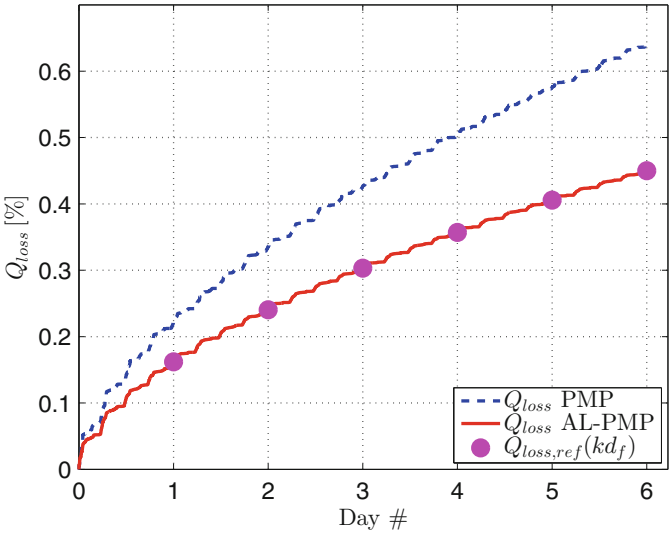

Fig. 9.40 Capacity loss profile over one week of simulation at $\theta_{\text{amb}} = 30°\text{C}$; comparison between reference values, results with standard PMP and with AL-PMP

the battery is needed. In Table 9.6 the results relative to the fuel consumption over the first week are shown. AL-PMP does not show a significant worsening in fuel economy when compared to PMP, showing that battery aging is much more sensitive to the choice of the control parameters than fuel consumption.

9.11 Conclusions

In this paper a new capacity loss model identified from real HEV data is adopted, from which a reference capacity loss profile is extracted and used in the multi-objective optimization strategy, referred to as AL-PMP. The AL-PMP is first formulated, and then solved with a new tuning algorithm. It is shown that both the state of charge and capacity loss are regulated to their respective reference values at the end of the first day of driving, at the price of a small increase in fuel consumption. For more severe driving conditions, a penalty function on capacity loss allows to obtain the same optimal results, but for extreme scenarios aging control is dominated by the uncontrolled charging phase. The same results obtained for the first day of driving are confirmed by simulations performed over an entire week of driving: both states are optimally controlled and the fuel consumption is comparable to that of a standard (i.e., that does not account for aging) control strategy.

Table 9.6 Fuel consumption obtained in simulation over the first week of driving at $\theta_{\text{amb}} = 30°\text{C}$: results for standard PMP and AL-PMP, and increase in fuel consumption of AL-PMP with respect to PMP

Day #	$m_f[kg]$ PMP	$m_f[kg]$ AL-PMP	Increase in $m_f[\%]$
1	2.4471	2.4573	0.417
2	2.4471	2.4696	0.922
3	2.4471	2.4717	1.008
4	2.4470	2.4721	1.022
5	2.4471	2.4724	1.036
6	2.4470	2.4727	1.050

As a possible future development of this work, in order to overcome the limitations of AL-PMP, two paths are proposed, to be integrated within the present solution:

- A simple approach is to apply a *rule-based* braking strategy, to limit the maximum braking power when temperature is above a certain safety threshold; in this way a milder aging effect will be obtained in charging and this will be sufficient to optimally meet the daily goal $Q_{\text{loss,ref}}(d_f)$, while maintaining charge-sustainability.
- Series braking, as implemented in this work, could be replaced by a more *ad hoc* parallel braking strategy with the purpose of optimizing recuperation as proposed in [25], and, at the same time, accounting for battery aging.

Acknowledgements The authors would like to acknowledge the support received from Honda R&D co., Ltd., Japan and they would also like to thank Girish Suri for the help in improving the vehicle simulator.

References

1. S. Onori, L. Serrao, G. Rizzoni, *Hybrid Electric Vehicles Energy Management Strategies* (Springer, Berlin/Heidelberg, 2016)
2. L. Guzzella, A. Sciarretta, *Vehicle Propulsion Systems: Introduction to Modeling and Optimization* (Springer, Berlin, 2007)
3. C. Chan, The state of the art of electric, hybrid, and fuel cell vehicles, Proc. IEEE **95**, 704–718 (2007)
4. F. Lewis, V. Syrmos, Dynamic programming, in *Optimal Control* (Wiley, New York, 1995), pp. 315–347
5. S. Onori, Model-based optimal energy management strategies for hybrid electric vehicles, in *Optimization and Optimal Control in Automotive Systems - Lect. Notes in Control Science*, ed. by H. Waschl, I. Kolmanovsky, M. Steinbuch, L. del Re (Springer, New York, 2014), pp. 199–218

6. R. Cipollone, A. Sciarretta, Analysis of the potential performance of a combined hybrid vehicle with optimal supervisory control, in *Computer Aided Control System Design, International Conference on Control Applications, International Symposium on Intelligent Control* (ASME, New York, 2006), pp. 2802–2807
7. R. Bellman, Dynamic programming and Lagrange multipliers, in *Proceedings of the National Academy of Sciences of the United States of America*, vol. 42, p. 767, 1956
8. L. Pontryagin, V. Boltyanskii, R. Gamkrelidze, E. Mischchenko, *The Mathematical Theory of Optimal Processes* (Interscience, New York, 1962)
9. A. Sciarretta, L. Guzzella, Control of hybrid electric vehicles - A survey of optimal energy-management strategies. IEEE Control Syst. Mag. 27, 60–70 (2007)
10. J. Kessels, M. Koot, P. Van den Bosch, D. Kok, Online energy management for hybrid electric vehicles. IEEE Trans. Veh. Technol. **57**, 3428–3440 (2008)
11. C. Musardo, B. Staccia, S. Midlam-Mohler, Y. Guezennec, G. Rizzoni, Supervisory control for NOx reduction of an HEV with a mixed-mode HCCI/CIDI engine, in *Proceedings of the American Control Conference*, vol. 6, 2005, pp. 3877–3881
12. N. Shidore, J. Kwon, A. Vyas, Trade-off between PHEV fuel efficiency and estimated battery cycle life with cost analysis, in *Vehicle Power and Propulsion Conference*. IEEE, 2009, pp. 669–677
13. S. Moura, J. Stein, H. Fathy, Battery health-conscious power management for plug-in hybrid electric vehicles via stochastic control, in *Dynamic Systems and Control Conference* (ASME, New York, 2010)
14. L. Serrao, S. Onori, A. Sciarretta, Y. Guezennec, G. Rizzoni, Optimal energy management of hybrid electric vehicles including battery aging, in *American Control Conference (ACC)*, 2011, pp. 2125–2130
15. L. Tang, S. Onori, G. Rizzoni, Optimal energy management of HEVs with consideration of battery aging, in *IEEE Transportation Electrification Conference and Expo (ITEC)*, 2014
16. S. Ebbesen, P. Elbert, L. Guzzella, Battery state-of-health perceptive energy management for hybrid electric vehicles. Trans. Veh. Technol. **61**, 2893–2900, 2012
17. J. Wang, P. Liu, J. Hicks-Garner, E. Sherman, S. Soukiazian, M. Verbrugge, H. Tataria, J. Musser, P. Finamore, Cycle-life model for graphite-$LiFePO_4$ cells. J. Power Sources, **196**, pp. 3942–3948, 2011
18. T. Pham, P. van den Bosch, J. Kessels, R. Huisman, Cost-effective energy management for hybrid electric heavy-duty truck including battery aging, in *Dynamic Systems and Control Conference (DSCC)*, 2013
19. G. Suri, S. Onori, A control-oriented cycle-life model for hybrid electric vehicle lithium-ion batteries. Energy **96**, 644–653 (2016)
20. M. Broussely, S. Herreyre, P. Biensan, P. Kasztejna, K. Nechev, R. Staniewicz, Aging mechanism in li ion cells and calendar life predictions. J. Power Sources **97–98**, 13–21 (2001)
21. S. Grolleau, A. Delaille, H. Gualous, P. Gyan, R. Revel, J. Bernard, E. Redondo-Iglesias, J. Peter, Calendar aging of commercial graphite/LiFePO4 cell - predicting capacity fade under time dependent storage conditions. J. Power Sources **255**, 450–458 (2014)
22. F. Todeschini, S. Onori, G. Rizzoni, An experimentally validated capacity degradation model for Li-ion batteries in PHEVs applications, in *8th IFAC International Symposium on Fault Detection, Supervision and Safety of Technical Processes* (2012)
23. S. Onori, P. Spagnol, V. Marano, Y. Guezennec, G. Rizzoni, A new life estimation method for lithium-ion batteries in plug-in hybrid electric vehicles applications, Int. J. Power Electron. **4**(3), 302–319 (2012)
24. 2009 National Household Travel Survey. Available: http://nhts.ornl.gov/2009/pub/stt.pdf [Online]
25. K. Bayar, R. Biasini, S. Onori, G. Rizzoni, Modelling and control of a brake system for an extended range electric vehicle equipped with axle motors. Int. J. Veh. Des. **58**, 399–426 (2012)

26. L. Serrao, S. Onori, G. Rizzoni, "ECMS as a realization of Pontryagin's Minimum Principle for HEV control, in *Proceedings of the American Control Conference* (IEEE Press, New York, 2009), pp. 3964–3969
27. A. Allam, S. Onori, S. Marelli, C. Taborelli, Battery health management system for automotive applications: a retroactivity-based aging propagation study, in *2015 American Control Conference (ACC)*, July 2015, pp. 703–716
28. A. Cordoba Arenas, S. Onori, Y. Guezzennec, G. Rizzoni, Capacity and power fade cycle-life model for plug-in hybrid electric vehicle lithium-ion battery cells containing blended spinel and layered-oxide positive electrodes J. Power Sources **278**, 473–483 (2015)